FE-2229-3
Distribution Category UC-90c

SURFACE STRUCTURE AND MECHANISMS OF GASIFICATION CATALYST DEACTIVATION

Quarterly Report for the Period
August – October 1976

P. J. Reucroft
E. B. Bradley
R. J. De Angelis
G. A. Sargent

UNIVERSITY OF KENTUCKY
Lexington, Kentucky 40506

Date Published
December 1976

PREPARED FOR THE UNITED STATES
ENERGY RESEARCH AND DEVELOPMENT ADMINISTRATION
Under Contract No. E(49-18)-2229

I. ABSTRACT

Experimental work is now underway in all four Task areas. The LEED-Auger system has been delivered and installed and preliminary studies to evaluate the capabilities of the Auger technique have been carried out.

The ESCA studies on the coprecipitated catalysts have continued. In this period, studies have dealt with the oxygen $1s_{1/2}$ spectra that can be observed in catalyst samples and nickel oxide standard samples. Corrected binding energies, which allow for sample charging effects, have been estimated for some of the standard samples.

Additional work has been carried out to develop computer programs for evaluating intensity variations in diffracted beams that arise due to different atom types in the surface structures to be investigated.

An x-ray diffraction technique has been developed which allows calculation of the coherent diffracting particle size and mean square strain from a single diffraction profile. The effective particle size, obtained for unreduced catalysts in the as received and sintered conditions by this method, are compared with those obtained from the half breadth of the profile and the initial slope of the Stokes' corrected cosine coefficients of the profile.

Infrared spectra of unreduced catalysts dispersed in a KBr matrix have been obtained and compared with similar data obtained for standard samples. It is concluded that a significant fraction of the nickel is in the form of a complex silicate in the silica supported catalysts.

II. OBJECTIVE AND SCOPE OF WORK

The objective of the program is to characterize the surface structure of methanation catalysts in order to relate structural features to catalytic activity and catalyst deactivation. Surfaces to be examined include (a) single crystal nickel with well-defined crystal planes and (b) dispersed samples of nickel and nickel alloys on alumina and silica supports. The chemical composition and surface concentration will be measured by ESCA and Auger Spectroscopy. Chemical bonding information will be determined by Raman and infrared spectroscopy. Structural changes in the surface lattice will be investigated by LEED characterization. The catalyst surface will be investigated in the presence of CO, H_2, CH_4 and H_2S in the initial stages of the program. Other potential poisons and deactivating agents, such as chlorides, cyanides, nitrogen oxides and carbon depositors such as ethylene and benzene will be investigated as the program develops. The validity of currently accepted models of catalyst thermal deactivation i.e. sintering, will be evaluated and assessed for accuracy and applicability. Parameters to be monitored include (a) particle size and particle size distribution, (b) the effect of temperature on particle size distribution, and (c) the effect of particle size distribution on the rate of thermal sintering.

III. SUMMARY OF PROGRESS TO DATE

Experimental facilities for the four project task areas have now been established. Coprecipitated nickel methanation catalysts, containing ∿50% nickel on an alumina or silica suppport, have been mainly investigated in the initial stages of the project. The surface chemical composition has been studied by ESCA. The catalyst infrared absorption spectra has been investigated in order to obtain information on the chemical bonding state of nickel. X-ray diffraction techniques have been employed to determine both the average nickel particle size and the particle size distribution. In the next phase, it is anticipated that studies on single crystal nickel substrates will be initiated employing the LEED technique. Auger spectroscopy will be used to monitor the surface cleanliness. After receipt of a high power laser source, which is now on order, laser Raman studies will be initiated on catalyst and single crystal surfaces.

A more detailed description of the activities in the four task areas follows. The program in the four task areas are approximately on schedule. The overall status of the project to date is illustrated in Figure III 1. The project costs are currently just below the budgeted level.

Personnel who have participated in the project, in addition to the co-principal investigators, include Dr. B. H. Davis (Summer Research Associate), Dr. P. Ganesan (Postdoctoral Research Associate), Dr. R. Shalvoy (Postdoctoral Research Associate) Dr. J. M. Stencel (Postdoctoral Research Associate), Dr. C. H. Huang (Postdoctoral Research Associate), Mr. L. A. Rice (Research Technician) and several graduate assistants.

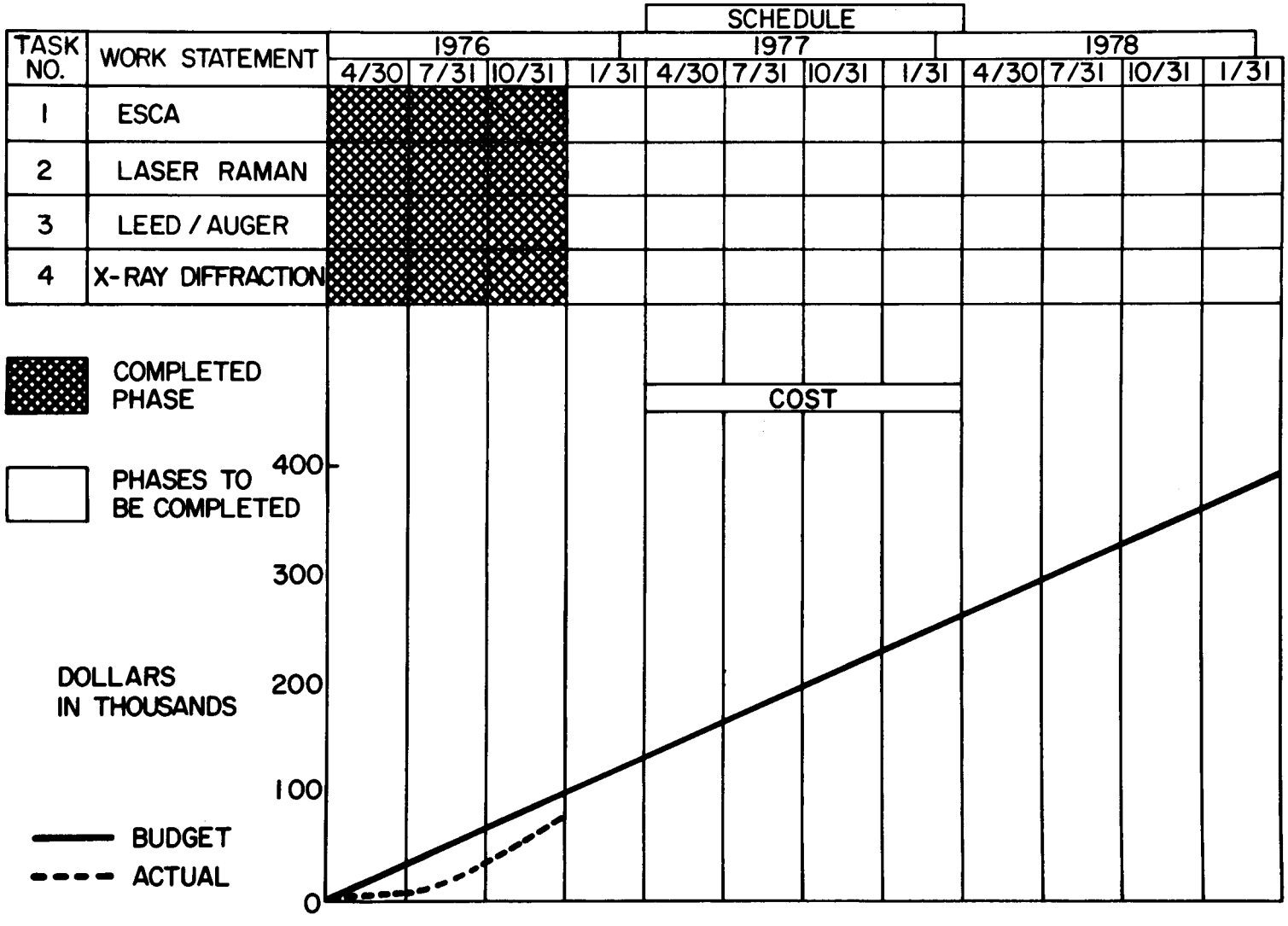

Fig. III 1: Summary of Project Progress

IV. DETAILED DESCRIPTION OF TECHNICAL PROGRESS

A. REPORTING CATEGORY 1 - ESCA STUDIES (Prepared by R. B. Shalvoy, B. H. Davis and P. J. Reucroft)

(i) Work Accomplished

In this period, the investigations that were described in Quarterly Report No. 2[1] have been continued further. Shifts in binding energy produced by surface charge have been determined to be in the range 1.5 - 3.9 eV, depending upon the system under investigation. Oxygen 1s spectra have been determined for several standard samples and catalysts of interest, and the effect of etching on the nickel $2p_{3/2}$ spectra has been evaluated for several catalyst specimens.

The catalysts currently under investigation in the four basic tasks are nickel coprecipitated methanation catalysts, in which the support material is either SiO_2 (C150-1-01 and C150-1-02) or Al_2O_3 (C150-1-03 and C150-4-03). The catalysts contain approximately 50% nickel (by weight) and are being investigated in both the reduced and pre-reduced forms. Studies have also been carried out on a "reduced and stabilized" form of the C150-1-01 catalyst. This sample was reduced and then subsequently exposed to air. Chemical and physical properties of these catalysts are described in Quarterly Report No. 1[2].

Instrumental Calibration

The ESCA instrument has now been recalibrated by a procedure that eliminates the systematic discrepancies between experimental and literature binding energies reported previously[1]. The calibration procedure was carried out as follows:

For aluminum radiation, a Mg foil sample was inserted in the spectrometer and the energy difference between the $1s_{1/2}$ and 2p peaks was measured. This difference should be 1253.6 eV[3]. The calibration of the spectrometer was then adjusted until the measured difference between these peak energies was equivalent to the predicted value within a tolerance of $\pm$ 0.1 eV. This insured that the voltage scale applied to the analyzer was the same as that assumed by the DS100 control program of the computer[4]. Fig. IV A1 of the last quarterly report verifies that this scale is linear[1].

The absolute value of the binding energy scale was then set by adjusting the work function of the DS100 control program so that the Au $4f_{7/2}$ peak had a binding energy of 84.0 eV[5] relative to the spectrometer Fermi level.

Following the recalibration, the binding energy of the nickel foil $2p_{3/2}$ peak and the binding energy of a series of lead peaks that had been previously determined were measured and found to agree with previously reported values[6,7]. The data obtained prior to the recalibration were all corrected by the procedure described previously[1], and may be directly compared with the results obtained after the recalibration.

Analysis of the Standard Samples

a) Chemical Analysis

It was observed previously that the Ni $2p_{3/2}$ spectra of the standard oxide samples (NiO, $Ni_2O_3 \cdot 6H_2O$, and NiO - Ni_2O_3) were very similar. Each spectrum consisted of two peaks separated by about 2.4 eV (Fig. IV A5 of reference 1). This called into question the actual chemical composition of these samples since the spectra indicated that both Ni (II) and Ni (III) oxide states were present in each sample.

A chemical analysis for bulk nickel content was performed. Samples were heated in air for two days at 650°C. The weight losses measured indicated that only the Alfa $Ni_2O_3 \cdot 6H_2O$ lost a significant amount of water. The results of the analysis are shown in Table 1. Samples were dried at 120°C and 650°C before analysis. From these data, the NiO and Alfa mixed oxide samples appear to be mainly NiO while the Apache mixed oxide sample appears to be mainly Ni_2O_3. These results are not easily reconciled with the ESCA data. The results indicate that while the bulk composition reflects the indicated composition of the material, the surface composition, as monitored by ESCA, is dominated by mixed oxide states independent of whether the bulk material is NiO, Ni_2O_3 or NiO - Ni_2O_3.

Figs. IV A1 and IV A2 show the Ni $2p_{3/2}$ and O $1s_{1/2}$ spectra respectively for $Ni_2O_3 \cdot 6H_2O$ calcined in air for 24 hours at 650°C and NiO prepared by decomposing $NiCO_3$ in air at 300°C. These spectra are similar to those of the standard samples. These spectra were investigated as a separate check on the composition of the standard samples.

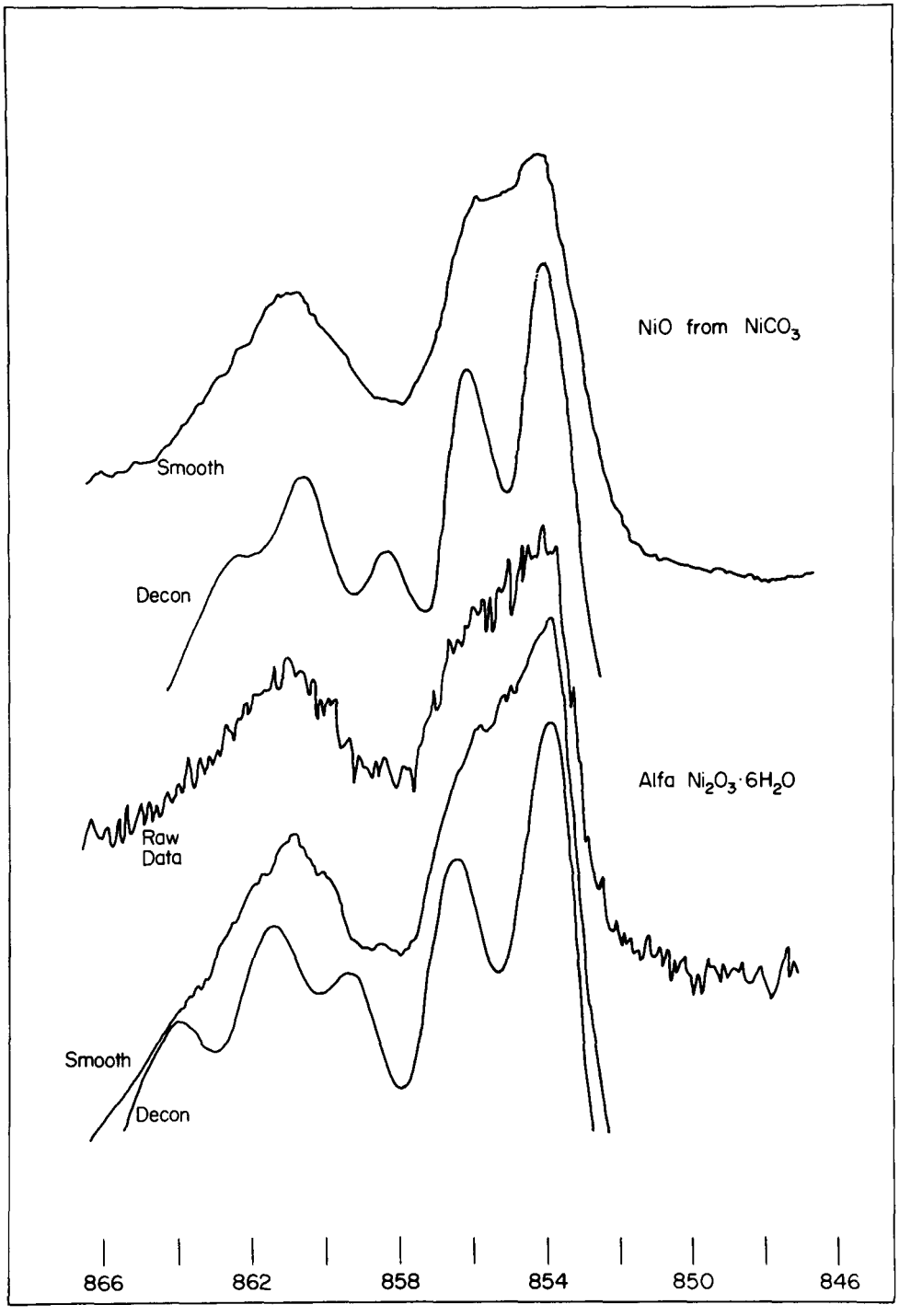

Fig. IV A1: ESCA spectra (Ni $2p_{3/2}$, smoothed, deconvoluted) of a NiO sample, prepared by decomposing $NiCO_3$, and of $Ni_2O_3 \cdot 6H_2O$, supplied by Alfa Inorganics.

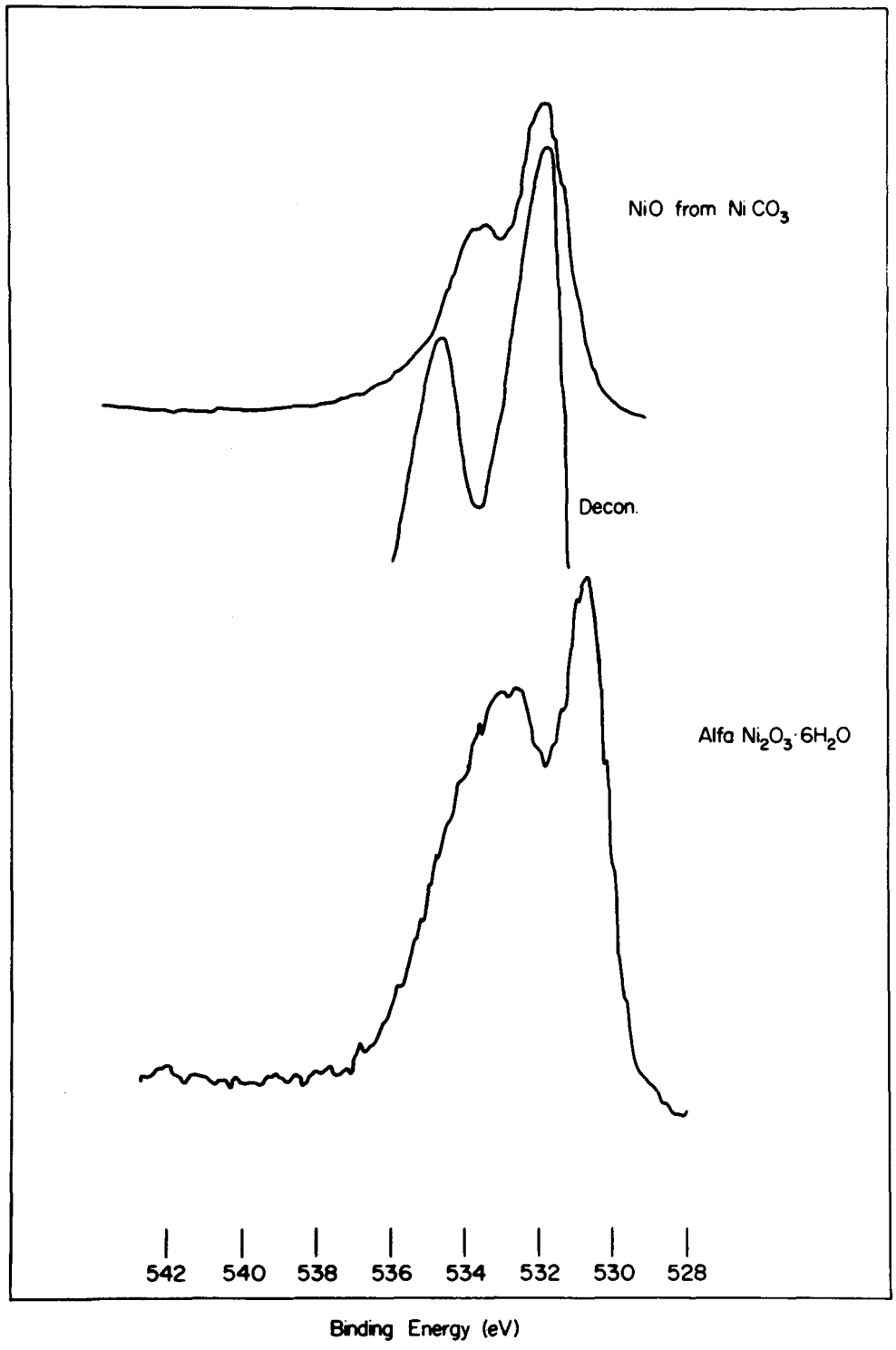

Fig. IV A2: ESCA spectra (0 $1s_{1/2}$) of a NiO sample, prepared by decomposing $NiCO_3$, and of $Ni_2O_3 \cdot 6H_2O$, supplied by Alfa Inorganics.

b) Oxygen 1s spectra

The oxygen $1s_{1/2}$ peak structure of the standard samples has also been investigated. The interpretation of the peak structure is more straightforward than that of the Ni $2p_{3/2}$ peak as the oxygen level has a significantly smaller natural width (full width at half maximum observed is about 1 eV as compared to 2.3 eV for the nickel metal peak). In addition, shakeup satellite peaks are absent. However, the interpretation may be complicated by the presence of adsorbed surface oxygen from CO or H_2O, which generally contributes a peak at binding energies of about 532 eV. This complication can be reduced by brief Ar ion etching, which reduces the contribution from these contaminants.

The samples of NiO and $NiO-Ni_2O_3$ give two peaks (Fig. IV A3) at slightly higher binding energies than those reported in the literature[7-9] (Fig. IV A4). The low binding energy peak is at about 530.4 eV and the high binding energy peak is at 532.7 eV. On the other hand, the peaks for $Ni_2O_3 \cdot 6H_2O$ are at lower binding energies than those reported in the literature. In all other respects, the oxygen 1s peaks are in excellent agreement with those reported in the literature. The similarity of the spectra of the three standard samples confirms the finding from the chemical analysis that the water of hydration has been lost. If we assign the lower binding energy peak to the oxide associated with the Ni (II) state and the higher peak to the Ni (III) state, the two peaks are in general agreement with the relative peak areas that were assigned to the two peaks observed in the Ni $2p_{3/2}$ spectra.

Both NiO and $NiO-Ni_2O_3$ samples were examined after argon ion etching. There was very little change in the O $1s_{1/2}$ spectra of either sample, indicating that the presence of adsorbed oxygen is not a major contributor to the observed oxygen spectrum in the case of these materials.

c) Sample Charging Effects

When insulating samples are investigated by the ESCA technique, sample charging can greatly complicate the observed spectra by altering the binding energies and widths of the core peak spectra[10]. The problem

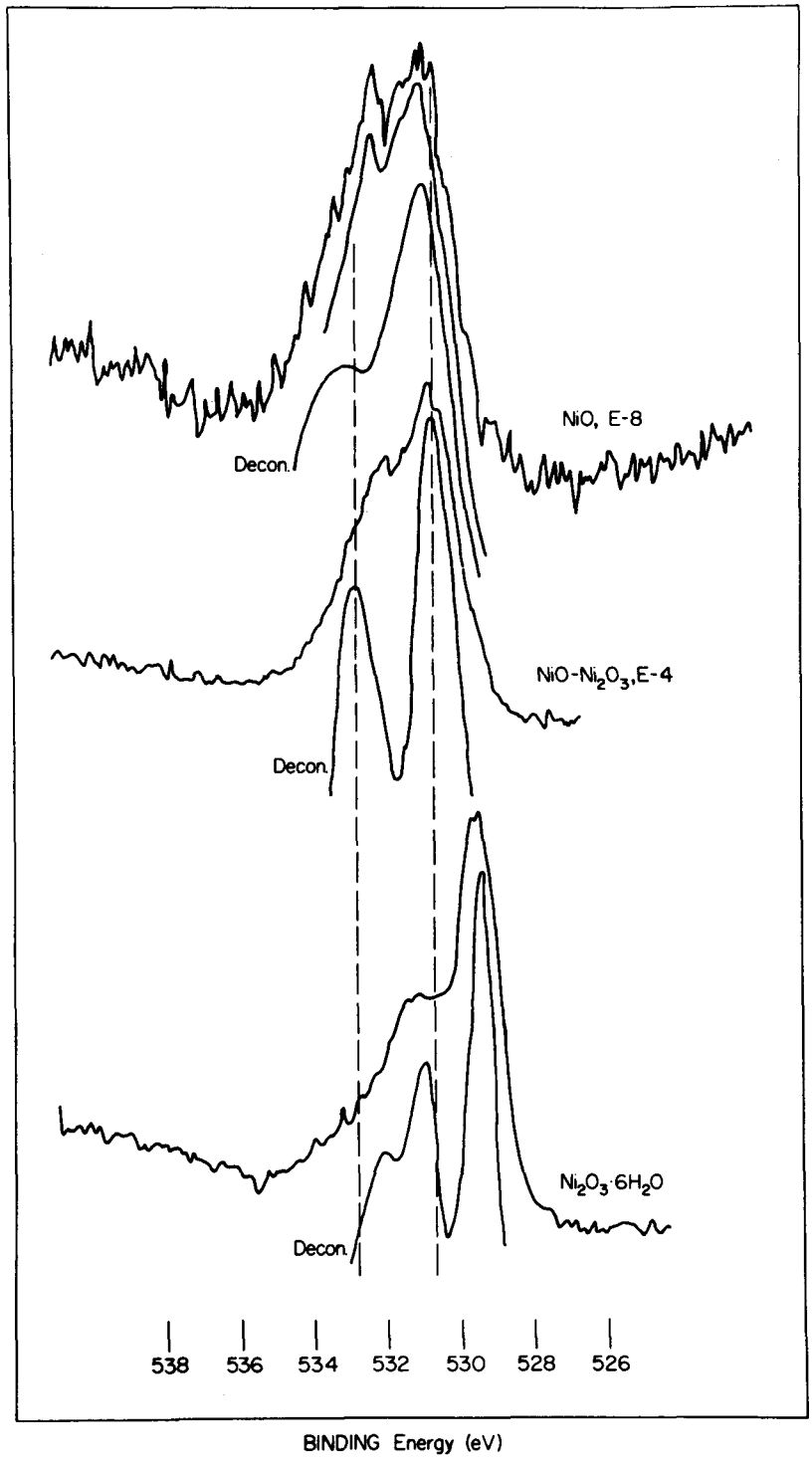

Fig. IV A3: ESCA spectra (O $1s_{1/2}$, experimental and deconvoluted) of the reference nickel oxide samples (NiO, Ni_2O_3 - NiO, $Ni_2O_3 \cdot 6H_2O$).

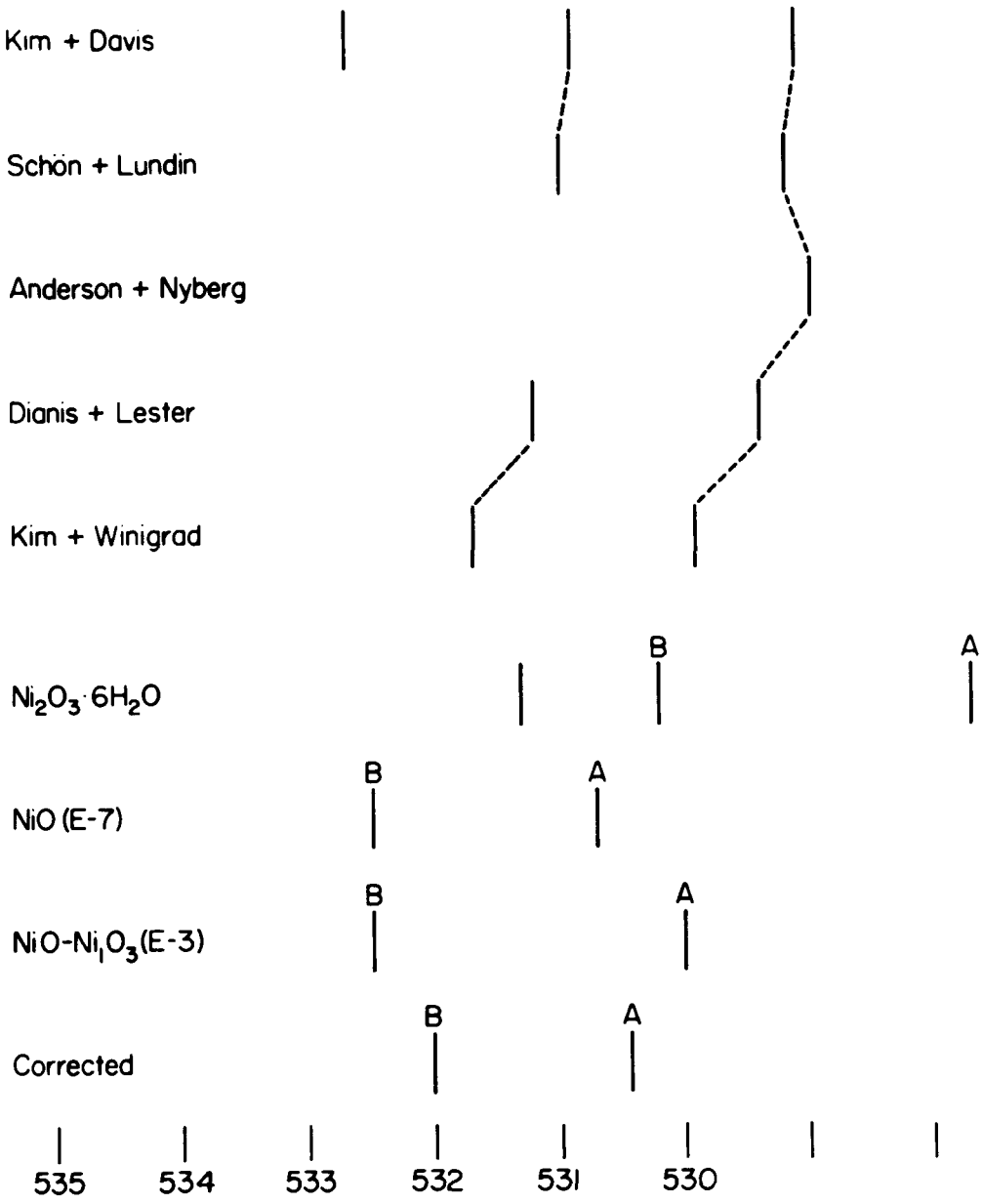

Fig. IV A4: Comparison of experimental ESCA oxygen $1s_{1/2}$ peak positions for the reference nickel oxide samples with some literature peak positions. Peak Positions after a charging correction are also indicated. Peaks A and B are attributed to the Ni (II) and Ni (III) oxides respectively.

may be attacked by two methods. The first approach involves neutralization of the surface charge created by the emission of photoelectrons, by flooding the sample surface with very low energy electrons. The second approach consists of determining the shift in binding energy produced by the surface charge and correcting the measured binding energies. The latter technique does not deal with the problem of peak broadening. Consequently, the resolution of the spectrometer still remains limited.

Binding energy shifts due to sample charging were determined in the following manner for several insulating samples of interest. Powder samples were mounted on conducting copper backed tape and a thin silver paint mix was spotted on the surface of the sample. The silver was in contact with the sample (but not the copper) and charge present on the surface shifted the binding energy of the silver peaks. Since the binding energy of silver (when grounded) is well known, any charge on the sample or drift of the analyzer could be detected and the sample binding energies could then be corrected. Nickel oxide spectra similar to those described in the last report[1] were obtained and the determined binding energy correction was 1.5 eV. Table 2 summarizes the corrected binding energies along with the corrected binding energies of some other compounds of interest. Given the uncertainty in the observed binding energies and the method of correcting for the charge, these energies are considered accurate to about $\pm$ 0.5 eV. Nickel aluminate and nickel carbonate will be evaluated in the next period. The peak widths observed were generally broad providing additional confirmation of surface charge effects.

TABLE 1. ANALYSIS OF NICKEL STANDARD SAMPLES

Alfa Ni (II, III)

Weight loss after heating for 2 days at 650°C was 0.48%

Apache Ni (II, III)

Weight loss after heating for 2 days at 650°C and 6.876%

Apache NiO

Weight loss after heating for 2 days at 650°C was 0.0716%

NICKEL ANALYSIS

Sample	% Ni, dry 120°C	% Ni, 650°C calcination
Ni (II), Apache	77.23; 78.33	Same as 120°C drying
Ni (II, III), Alfa	77.56; 76.89	77.95; 77.28
Ni (II, III), Apache	65.32	70.14

% Ni calculated for pure: NiO = 78.58

Ni_2O_3 = 70.98

Weight loss for $Ni_2O_3 \cdot 6H_2O$ Samples

Apache Sample No weight loss after six (6) hours at 200°C.
Lost 0.838% weight after heating at 650°C for 24 hours.

Alfa Sample Lost 22.92% weight after heating at 650°C for 24 hours.

$$Ni_2O_3 \cdot 6H_2O = Ni_2O_3 + 6H_2O$$

Weight loss for above reaction would be 39.5%

$$Ni_2O_3 = 2NiO$$

Weight loss for above reaction would be 9.67%

Based on the weight loss of 39.5% for the first equation above, the Apache sample was 2.1% $Ni_2O_3 \cdot 6H_2O$, the Alfa sample was 58% hexahydrate.

TABLE 2. CORRECTED BINDING ENERGIES (All binding energies and shifts in eV)

Peak Observed	Nickel Oxide (Shift = 1.5)		Peak Observed	Nickel Silicate (Shift = 3.3)
	Ni(II)	Ni(III)		
Ni $2p_{3/2}$	855.2	857.5	Ni $2p_{3/2}$	856.7
			Ni 3p	69.2
O $1s_{1/2}$	530.5	532.0	O $1s_{1/2}$	532.5
			Si $2s_{1/2}$	154.6

Peak Observed	Al_2O_3 (Shift = 3.9)	Peak Observed	SiO_2 (Shift = 3.3)
Al $2s_{1/2}$	118.8	Si $2s_{1/2}$	153.6
Al 2p	74.0	Si 2p	102.6
O $1s_{1/2}$	531.3	O $1s_{1/2}$	532.2

C-150 Catalysts Spectra

a) Oxygen 1s spectra

Fig. IV A5 shows spectra obtained for the C-150-1-01 catalyst in the oxidized form and in the reduced and stabilized form (reduced in hydrogen and then exposed to air), nickel silicate, nickel oxide, and SiO_2. The silica peak is quite narrow. This is expected since silica contains only one type of oxygen. The silica oxygen peak is located at a much higher binding energy than that observed for the nickel oxides, consistent with the greater degree of covalent bonding in silica. The peak for nickel silicate resembles that of pure silica and is almost as narrow as that of the silica peak. However, the peak for C-150-1-01 (oxidized form) is at a lower binding energy and is much broader than the nickel silicate peak; this suggests that more than one type of oxygen is present. The spectrum will be re-examined in the next period since the full binding energy range was not evaluated in the preliminary result shown. After C-150-1-01 was reduced and stabilized by treatment with air, the oxygen spectrum was altered. A portion of the spectrum appears at about the same binding energy as the oxygen peak in nickel silicate. However, the reduced and stabilized oxygen $1s_{1/2}$ peak consists of several peaks and there is also a small peak at approximately 530.5 eV, which is in the region of the nickel oxide $1s_{1/2}$ oxygen peak.

Fig. IV A6 shows the O $1s_{1/2}$ spectra obtained for the C150-1-03 and C150-4-03 catalysts (in the oxidized form) and nickel aluminate. The nickel aluminate was prepared by adding nickel nitrate to a solution of potassium aluminate (much less than the theoretical nickel was added). The resulting precipitate was washed with distilled water, dried at 120°C and then calcined at 400°C for six hours in air. The sample so prepared contained potassium as an impurity. There is a consistent trend in the oxygen spectrum for the two C-150 catalyst samples. C-150-1-03 contains 47% Ni and the oxygen peak is at a higher binding energy than that observed for the higher Ni containing C-150-4-03 (56% Ni). The higher Ni containing catalyst appears to have at least two, and probably three, types of oxygen; the higher binding energy peak is near the position of the C-150-1-03 peak while the lower binding energy peak is close to the peak position observed in the case of nickel oxide.

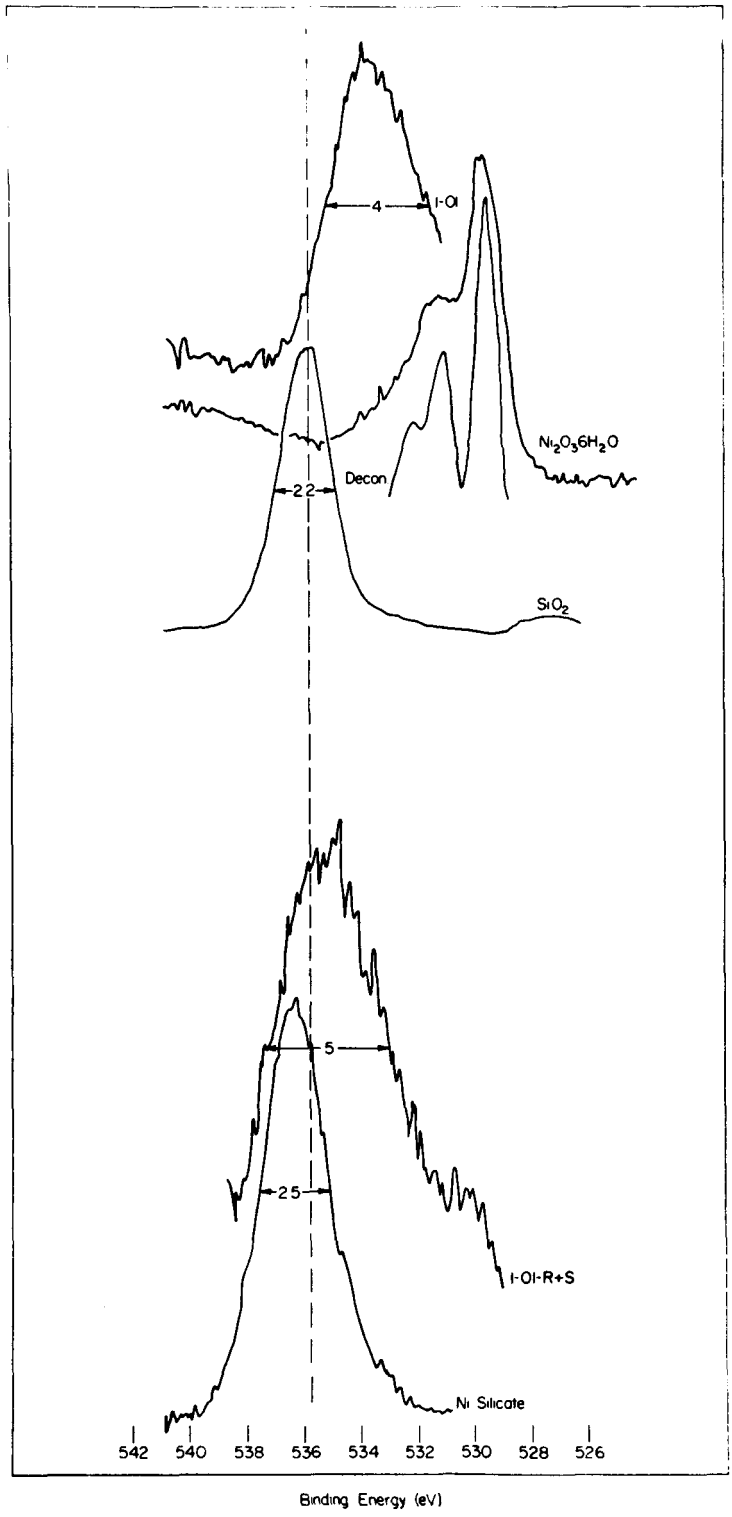

Fig. IV A5: ESCA spectra (0 $1s_{1/2}$) of the C150-1-01 and C150-1-01 R + S catalysts. The 0 $1s_{1/2}$ peaks of $Ni_2O_3 \cdot 6H_2O$, SiO_2, and nickel silicate are shown for comparison.

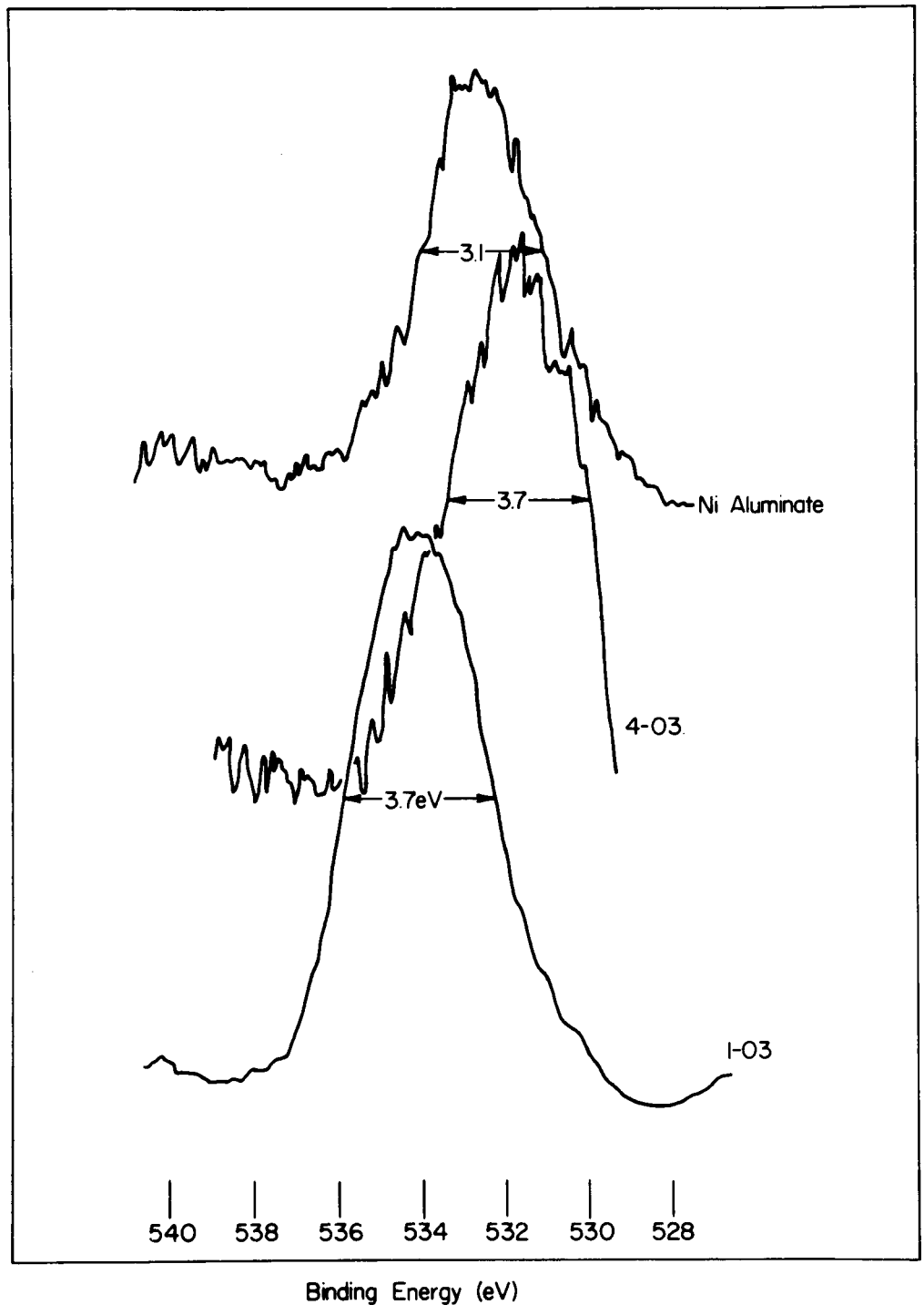

Fig. IV A6: ESCA spectra (0 $1s_{1/2}$) of nickel aluminate and two alumina based catalysts (C150-1-03 and C150-4-03).

b) Ion Etching studies on the C150-1-02, C150-1-03 and C150-4-03 catalysts

The 4-03 and 1-02 catalysts were studied in oxidized and reduced forms. Each sample was etched for an extended time period in a manner similar to that detailed previously.[1] Fig. IV A7 shows the Ni $2p_{3/2}$ spectrum for the 4-03 sample before reduction and after reduction (the reduction was carried out at 375°C for 16 hours in a 50% H_2-50% N_2 gas stream). The etching procedure is detailed in Table 3. After reduction, the major peak occurs at 857.2 eV(a in Fig. IV A7). After etching, two peaks appear in this region, one at about 858.5 - 859.5 eV and the other at 860.5 - 861.5 eV. Peaks due to nickel oxides are probably present, but do not become dominant. Prolonged etching revealed the nickel metal peak. Fig. IV A8 shows the O $1s_{1/2}$ spectra for this material. The peak is broad and the reduced sample shows a higher binding energy component. The sample does not appear to be either an aluminate or oxide.

The nickel spectra of the 1-02 sample are shown in Fig. IV A9. The unreduced material has a peak at 860.5 eV. This is the same value (uncorrected) as that reported for the nickel silicate sample. The reduced and etched (Table 4) samples did not show evidence of nickel metal, however. As the etching conditions become severe toward the end of the etch program, this is further evidence that the nickel metal peak that has been observed in the spectra is due to metal present in the catalyst and not metal formed by the etching procedure. The peaks, however, appear at different binding energies from those observed in the case of the 1-01 reduced and stabilized sample.[1]

Fig. IV A10 shows the O $1s_{1/2}$ spectra for the 1-02 catalyst. The observed peak is at the same position as oxygen in SiO_2. The silicon 2p peak also occurs at the same energy as that observed in SiO_2. The oxygen peak of the reduced and etched sample is similar to that of the unreduced sample. However, the reduced sample has a broader peak with a more pronounced low binding energy contribution which was intensified by etching. The 1-02 catalyst appears to show an appreciable nickel silicate character.

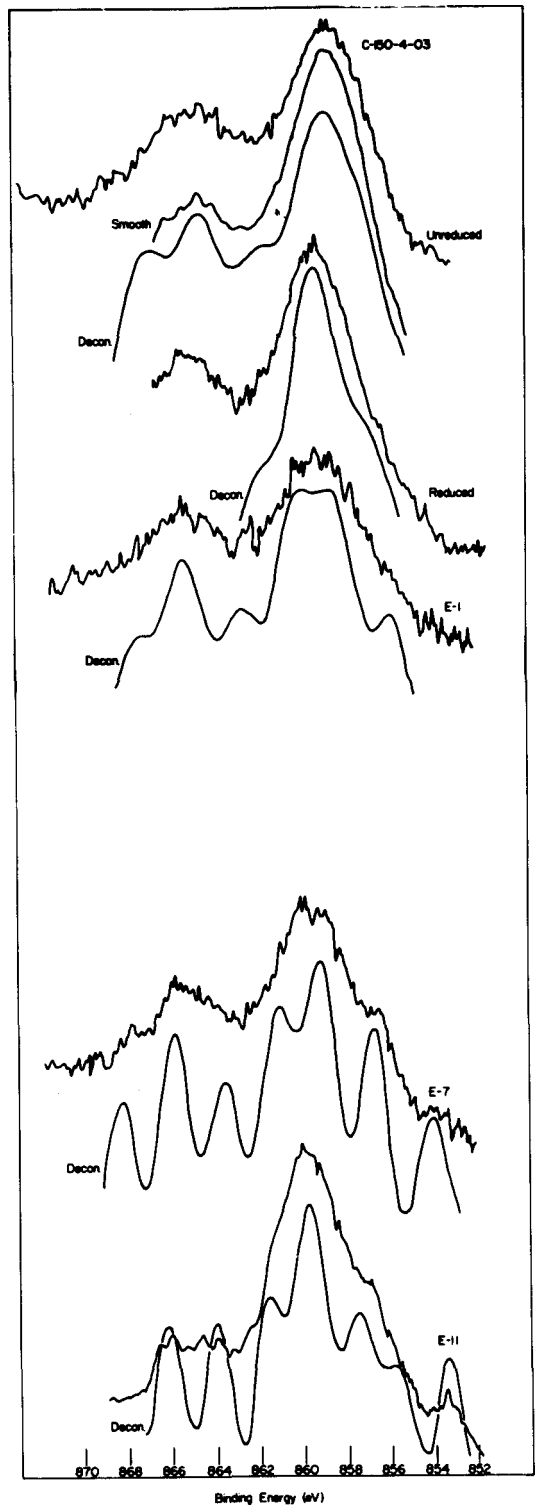

Fig. IV A7: ESCA spectra (Ni $2p_{3/2}$, experimental, smoothed and deconvoluted) of the C150-4-03 catalyst in unreduced and reduced forms, and after the subsequent argon ion etching program.

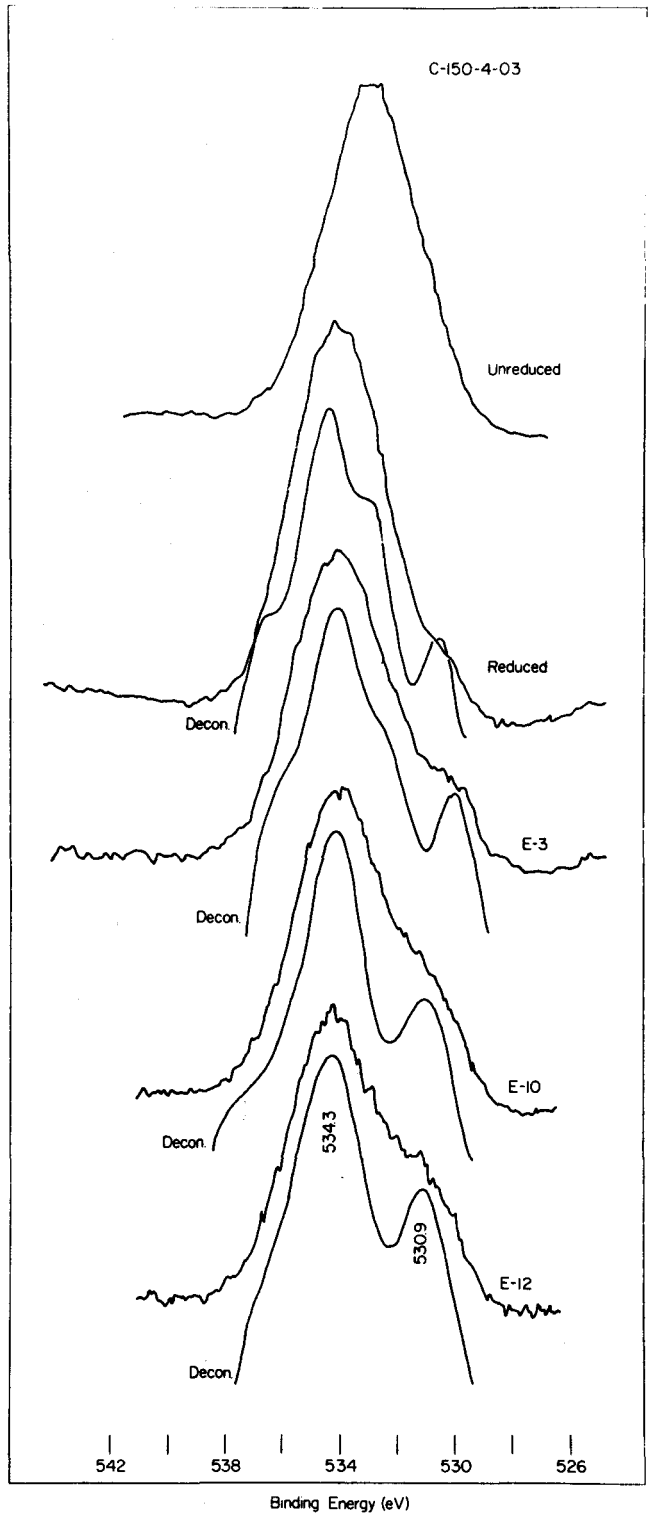

Fig. IV A8: ESCA spectra (O $1s_{1/2}$, experimental and deconvoluted) of the C150-4-03 catalyst in unreduced and reduced forms, and after the subsequent argon ion etching program.

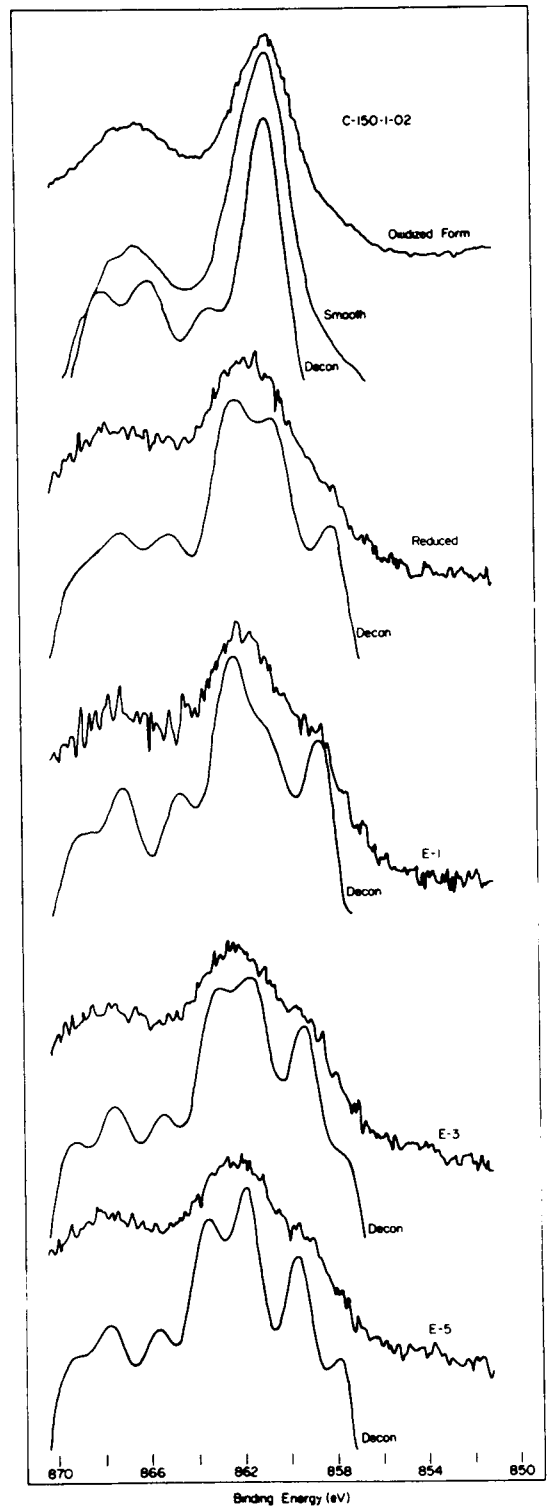

Fig. IV A9: ESCA spectra (Ni $2p_{3/2}$, experimental, smoothed, and deconvoluted) of the C150-1-02 catalyst in unreduced and reduced forms, and after the subsequent argon ion etching program.

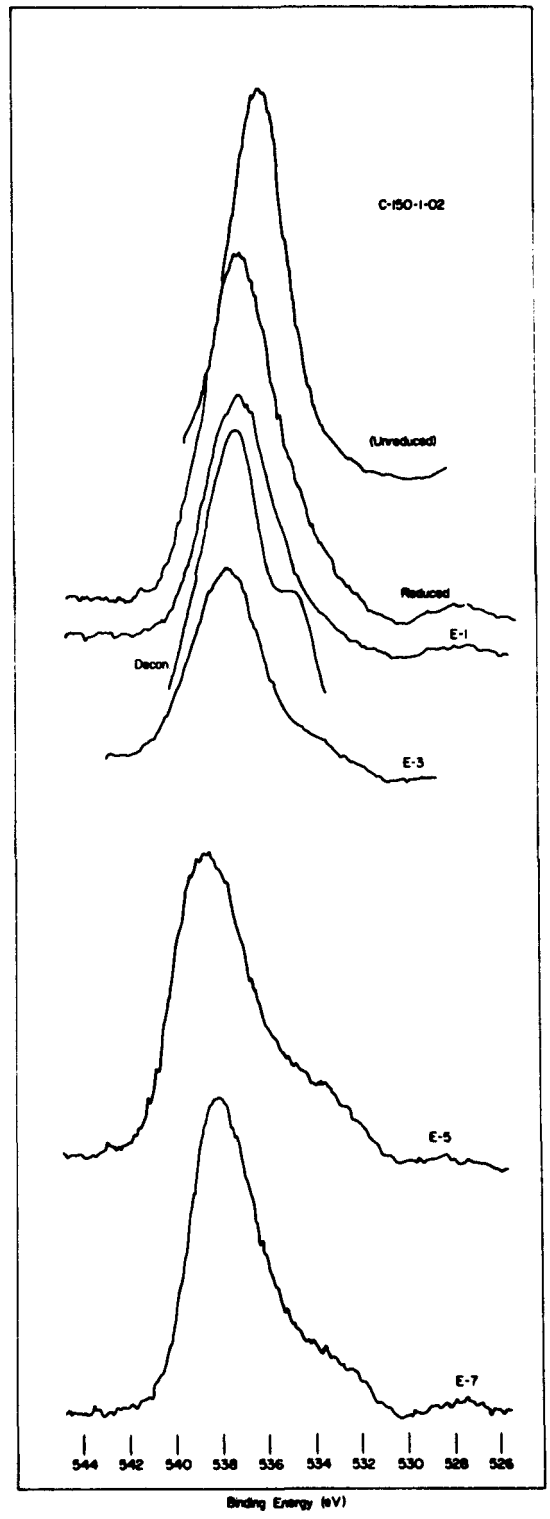

Fig. IV A10: ESCA spectra (O $1s_{1/2}$, experimental and deconvoluted) of the C150-1-02 catalyst in unreduced and reduced forms, and after the subsequent argon ion etching program.

TABLE 3. ARGON ION ETCH CONDITIONS FOR FIGURE IV A7. (Argon Pressure 5 x 10^{-6} Torr.)

	Etch Time (min)	Accumulated Etch Time (min)	Voltage (kV)	Current (mA)
E1	5	5	0.5	10
E2	8	13	0.5	20
E3	7	20	0.5	20
E4	10	30	0.5	20
E5	15	45	0.5	20
E6	5	50	1	10
E7	5	55	1	15
E8	7	62	1	15
E9	10	72	1	15
E10	10	82	1	20
E11	20	102	1	20
E12	8	110	1.5	15
E13	25	135	0.5	10

The spectra shown in Figure IV A7 were recorded after E1, E7 and E11 respectively.

TABLE 4. ARGON ION ETCH CONDITIONS FOR FIGURE IV A9. (Argon Pressure 5 x 10^{-6} Torr.)

Etch	Etch Time (min)	Accumulated Etch Time (min)	Voltage (kV)	Current (mA)
Before first run*	2	2	0.5	10
E1	10	12	0.5	15
E2	10	22	0.5	15
E3	8	30	0.5	20
	5	35	1.0	15
E4	9	44	1.0	15
E5	20	64	1.0	20
E6	20	84	1.0	20
E7	20	104	1.5	20

*Sample was in the high vacuum system for two days before sample was run.

The spectra shown in Figure IV A9 were recorded after E1, E3 and E5 respectively.

Fig. IV All is a comparison of spectra obtained for the reduced 1-02, 4-03 catalysts and the 1-01 (R + S) catalyst after the final etch procedure recorded in the appropriate tables. It is noteworthy that although the nickel silicate and nickel aluminate samples gave different nickel peak positions, the 1-01 R + S and 4-03 samples have almost identical peak positions. Differences observed between spectra obtained for the two silica supported catalysts (1-02 and 1-01 R + S) are not readily explained. However, it is apparent that if the 1-02 sample peaks are shifted by 1.7 eV to lower binding energies, the peak positions almost coincide with those of the other two samples. This indicates that surface charging to different degrees may be a problem in the case of the catalysts as well. Characterization of charging effects on the catalysts while they are being etched is more complicated than a determination of binding energy shift due to surface charge on standard samples. This problem is now under consideration. The problem lies primarily in finding a probe (e.g. such as the silver employed in the evaluation of the standard samples) that will not be effected by the etching procedure. Alternately, it may be assumed that the charging effect is independent of etching for a given sample. If this assumption is valid the charge effect can be evaluated by measuring binding energies either at the end or the beginning of an investigation. This point will be investigated in the next period.

The failure to observe nickel metal in some of the catalysts that were reduced immediately prior to the investigation,[1] may be due either to reoxidation during the sample transfer into the spectrometer, or to insufficient initial reduction. The reduction period has been increased from 16 to 32 hours and appears to adequately reduce the sample. Steps have been taken to reduce or eliminate the sample exposure to oxygen after the reduction bv performing the final sample transfer to the spectrometer probe inside a glove bag filled with oxygen free nitrogen gas. Alternate approaches include making the final transfer inside a more carefully evacuated glove box attached to the spectrometer or actually reducing the sample in a chamber attached to the spectrometer. The latter approach is the most desirable procedure and is currently being explored.

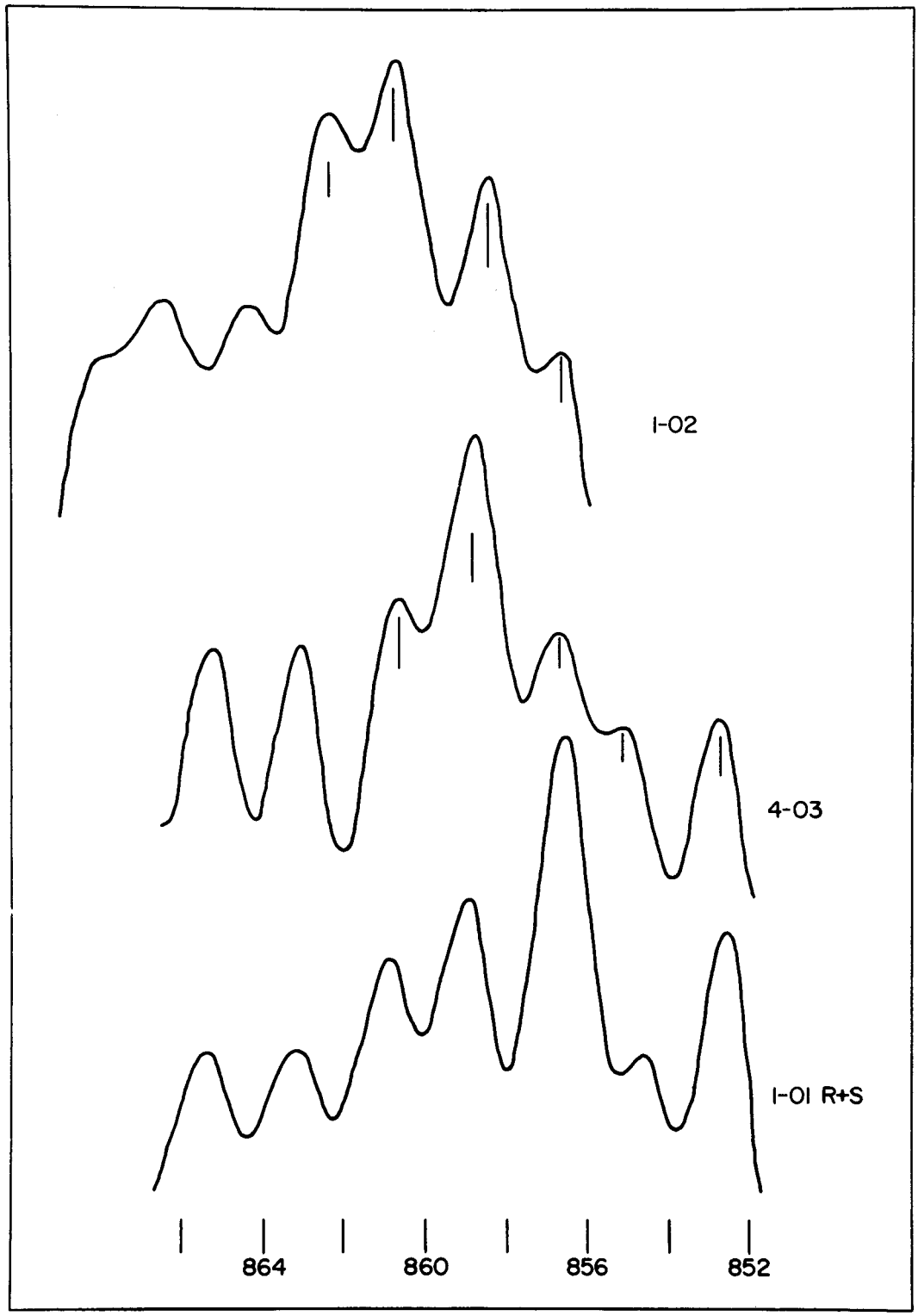

Fig. IV A11: Comparison of ESCA (Ni $2p_{3/2}$, deconvoluted) spectra of the C150-1-02, C150-4-03 and C150-1-01 R + S catalysts.

A preliminary investigation on a C150-1-03 sample was carried out employing the modified sample handling procedure and the longer reduction period. The sample was etched repeatedly (Table 5) but no nickel metal was observed. Fig. IV A12 shows the nickel and oxygen peaks before and after the etch program. This procedure will be refined further and attempted on the sample for which nickel metal was observed before deciding on the need for a separate reduction chamber.

Summary

Binding energy shifts due to surface charging appear to be ~1.5 eV in the case of nickel oxide standard samples. The standard samples appear to be mainly mixed nickel oxides in surface regions of the sample. Corrected binding energies for the Ni (II) and Ni (III) states have been tabulated along with the corrected binding energies of elements in some compounds of related interest. Binding energy shifts due to charging in Al_2O_3 and SiO_2 samples appear to be more significant than in the case of the nickel oxides.

The oxygen spectra of the standard samples confirm the two state character of the standard oxide samples. The presence of adsorbed oxygen does not appear to be a problem in interpreting these spectra.

Some of the reduced catalyst samples indicate that much of the nickel is present in forms other than metallic nickel. The nickel peak positions for the two oxide states and the silicate are closer together than was first reported, but are widely enough separated (approx. 1 eV between each) to allow ready identification of each state. Problems associated with charging and re-oxidation of samples complicate the interpretation of the catalysts' ESCA spectra. These problems are currently under study.

(ii) Work Forecast

1. Charging effects in standard samples of interest such as nickel aluminate and carbonate will be evaluated. Charging effects in the catalyst samples will be further investigated and a final interpretation of the untreated and reduced catalyst samples will be developed. The presence of silicate or aluminate will be verified.

2. Improved sample handling and mounting techniques will be developed in order to eliminate the possibility of sample re-oxidation.

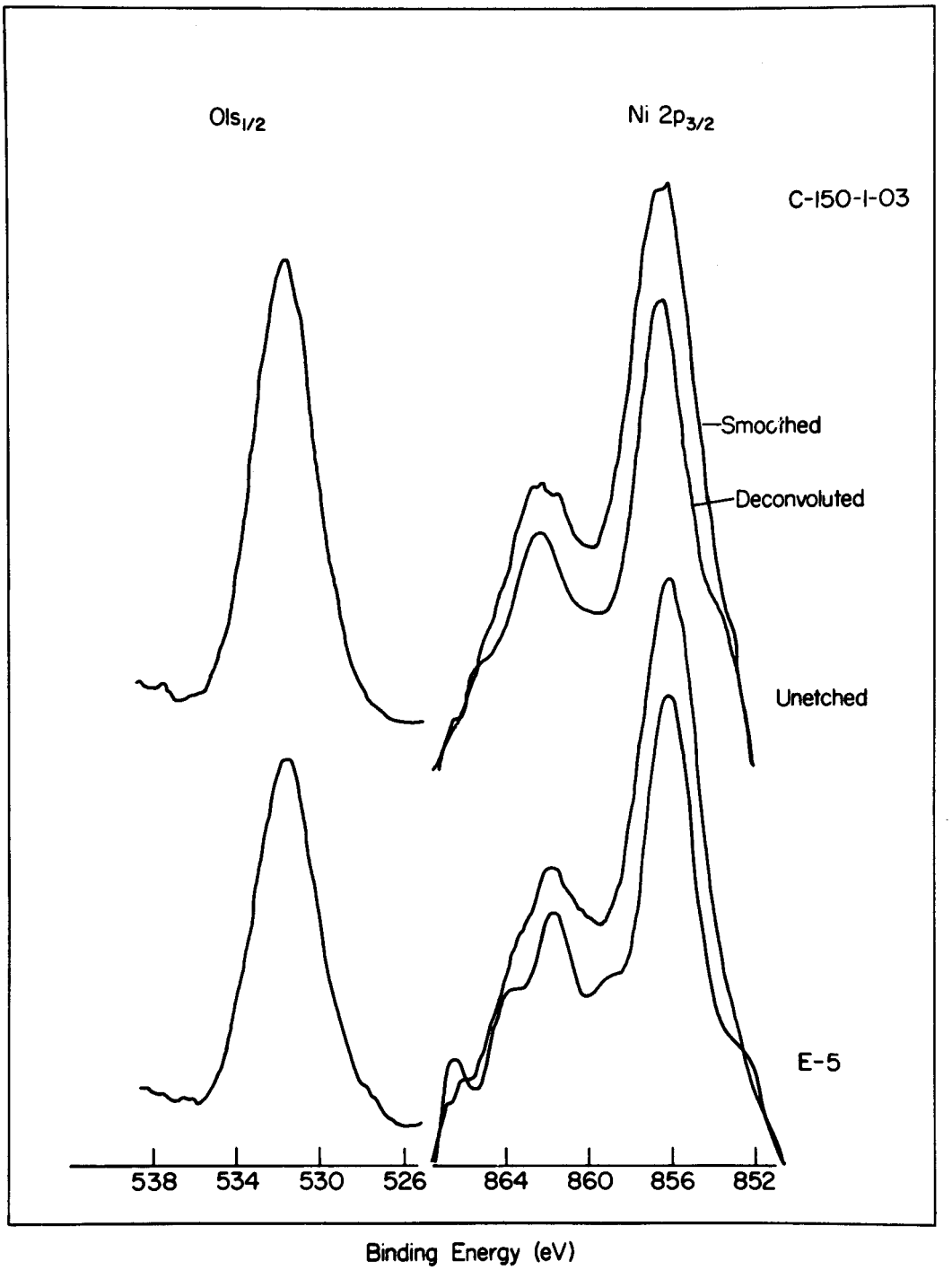

Fig. IV A12: ESCA spectra (O $1s_{1/2}$ and Ni $2p_{3/2}$) of the C150-1-03 catalyst in reduced form before argon ion etching and after E-5 of the etch program. This sample had been given special sample handling as explained in the text.

TABLE 5. ARGON ION ETCH CONDITIONS FOR FIGURE IV A12. (Argon Pressure 5 x 10^{-6} Torr.)

	Etch Time (min)	Accumulated Etch Time (min)	Voltage (kV)	Current (mA)
E1	3	3	1	20
E2	7	10	1	20
E3	12	22	1	20
E4	20	42	1.5	20
E5	30	72	2.0	20

3. A series of catalyst samples with lower nickel contents than the C150 series will be examined. The lower nickel content samples should show a higher concentration of silicate or aluminate if these compounds are forming. Some used and spent catalysts will also be examined and their natures characterized and related to the exposure given each.

4. Plans for the gas exposure experiments will be refined and preliminary studies will be carried out if suitable catalyst samples can be obtained.

(iii) References

1. P. J. Reucroft, E. B. Bradley, R. J. De Angelis and G. A. Sargent. Quarterly Report No. 2, "Surface Structure and Mechanisms of Gasification Catalyst Deactivation," May 1 to July 31, 1976, ERDA Contract NO. E(49-18) 2229.

2. P. J. Reucroft, E. B. Bradley, R. J. De Angelis and G. A. Sargent, Quarterly Report No. 1, "Surface Structure and Mechanisms of Gasification Catalyst Deactivation," February 1 to April 30, 1976, ERDA Contract No. E(49-18) 2229.

3. H. Fellner-Feldegg, U. Gelius, B. Wamberg, A. G. Nilsson, E. Basilier, and K. Siegbahn, J. Electron Spect. 5, 645 (1974).

4. Further details are given in the AEI ES 200 Instruction Manual.

5. I. Lindau, P. Pianetta, K. Y. Yu and W. E. Spicer, Physical Review B 13, 492 (1976).

6. L. Ley, R. Pollak, S. Kowalczyk and D. A. Shirley, Phys. Lett. 41A, 429 (1972).

7. K. S. Kim and R. E. Davis, J. Electron Spect. 1, 251 (1972/73).

8. G. Schon and S. T. Lundin, J. Electron Spect. 1, 105 (1972/73).

9. W. Dianis and J. R. Lester, Surf. Sci. 43, 602 (1974).

10. J. S. Brinen, J. Electron Spect. 5, 377 (1974).

B. REPORTING CATEGORY 2 - LASER RAMAN AND INFRARED SPECTROSCOPY (Prepared by J. Stencel and E. Bradley)

(i) Work Accomplished

In this period the investigation has focussed on identifying and assigning the infrared absorption bands of the catalysts in the 400 to 4000 cm^{-1} region. This has been accomplished by comparing the catalyst spectra to the spectra of their basic components and to published spectra. The pressed pellet technique was used in obtaining suitable infrared samples of these compounds[1].

Al_2O_3

Fig. IV B1 shows the infrared spectra of Al_2O_3 dispersed in a KBr pellet. It also shows the resulting spectra when the pellet had been heated to 300°C for approximately 24 hours.

The broad, intense absorption centered at 3450 cm^{-1}, and the absorption band at 1640 cm^{-1}, are due to the stretching and bending vibrations of trapped H_2O. Evidently the H_2O is tightly held in the KBr/Al_2O_3 matrix since continuous heating at 300°C did not appreciably decrease the intensity of the H_2O bands from that shown in Fig. IV B1 (2). The weak, narrow 1380 cm^{-1} band and the broad band centered at 2070 cm^{-1} disappear upon heating. These bands are thought to be due to CO vibrations of a carbonate-like species, which is generated in-situ from atmospheric CO_2 and H_2O during grinding and pressing of the KBr pellet.[2] The low frequency region (1300-400 cm^{-1}) shows two very broad, very intense bands centered at approximately 800 and 600 cm^{-1}. These are associated with Al-O vibrations, the nature of which can be discerned only by comparison with published spectra.

The transmission and reflection spectra of α - Al_2O_3 and ruby show strong absorption in the 800-670, 600 and 450 cm^{-1} regions.[3] Kolesova, et al.[4] report the spectra of $Al(OH)_3$ which has intense absorption in the 800 and 600 cm^{-1} regions, and OH deformation absorption at approximately 1000 cm^{-1}. Tarte has published the infrared spectra of θ - Al_2O_3 which is an aluminate consisting of condensed AlO_4 tetrahedra.[5] Plyusnia has given the spectra of $H_2O \cdot Al_2O_3$, which should have both tetrahedrally- and octahedrally-coordinated Al.[6] The last two publications show spectra which resemble our Al_2O_3 spectra both in spectral detail and absorption frequencies.

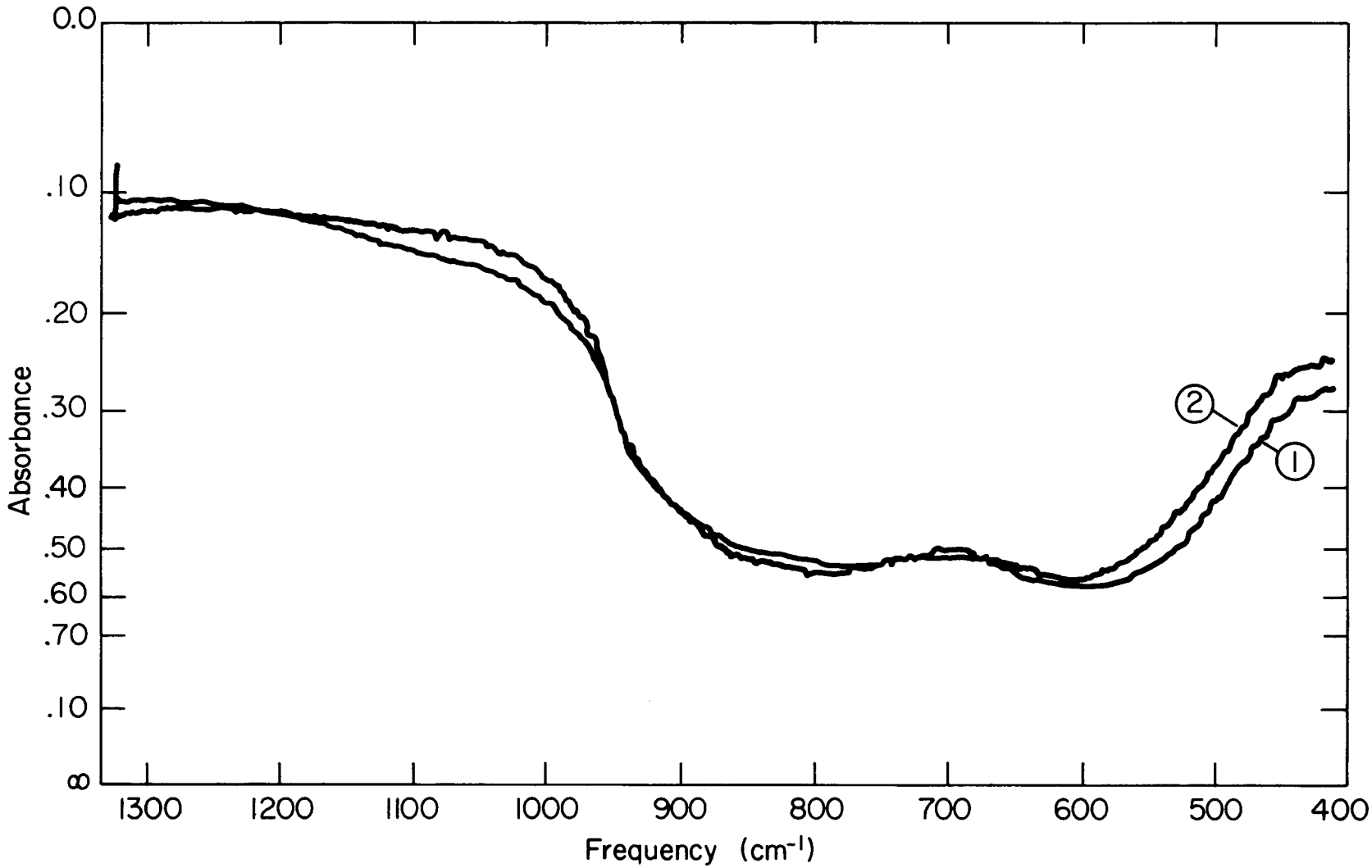

Fig. IV B1: (1) Infrared spectrum of Al_2O_3 dispersed in a KBr pellet, 1300-400 cm^{-1}.
(2) Al_2O_3 /KBr pellet spectrum after heating at 300°C for 24 hours.

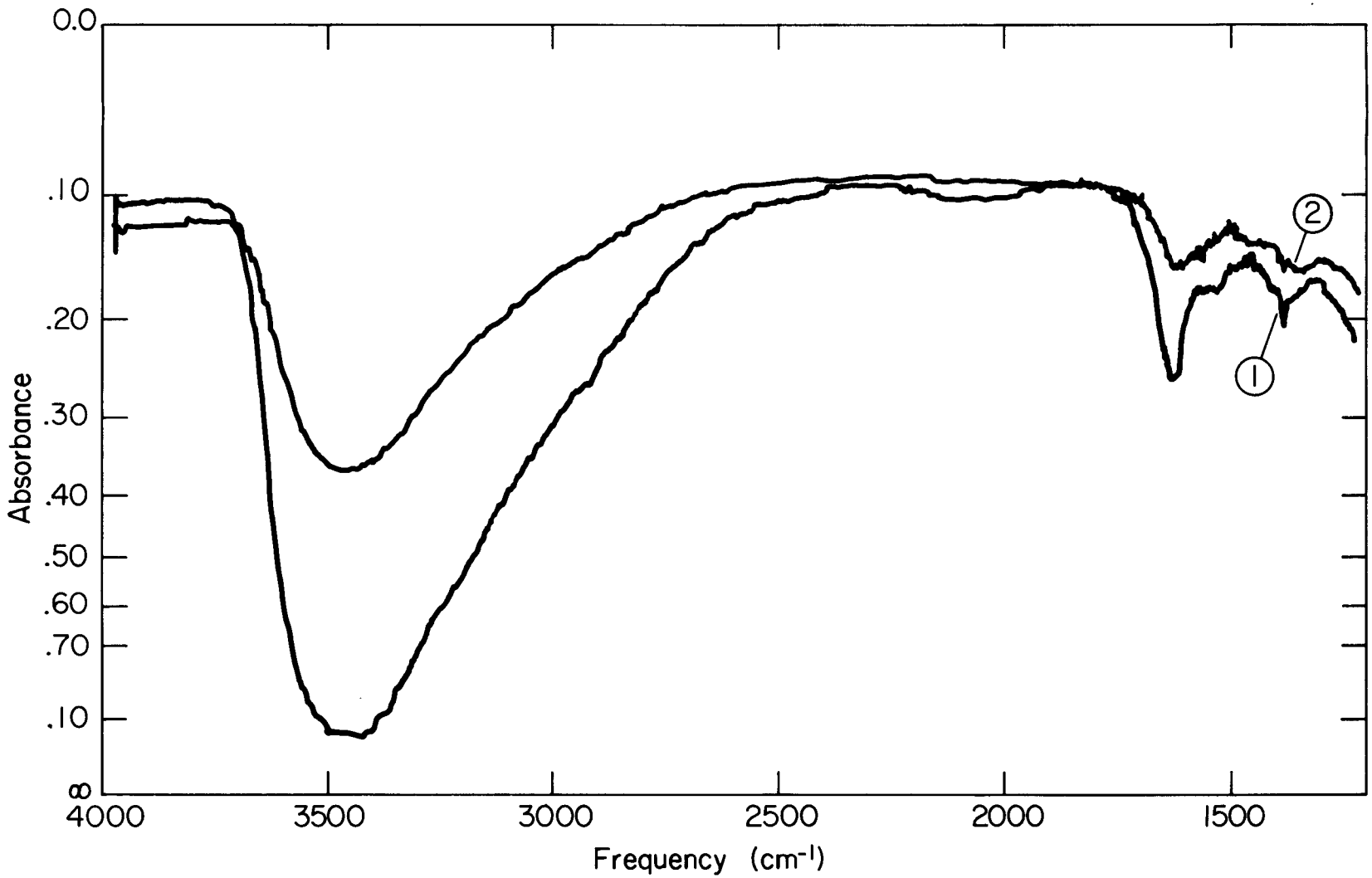

Fig. IV B1: (1) Infrared spectrum of Al_2O_3 dispersed in a KBr pellet, 4000-1300 cm^{-1}.
(2) Al_2O_3 /KBr pellet spectrum after heating at 300°C for 24 hours.

It is thought that the tightly-held H_2O broadens the Al-O absorptions through hydrogen bonding. Our Al_2O_3 samples could then be qualitatively described by the sheet-tetrahedrally coordinated aluminate $H_2O \cdot Al_2O_3$.

C150-4-03

This CCI catalyst contains the largest percentage of Ni of the methanation catalysts and an alumina support. Its spectra is shown in Fig. IV B2.

The high-frequency region (4000-1200 cm^{-1}) shows H_2O absorption centered at 3475 and 1650 cm^{-1}. The heating of the sample pellet at 300°C causes these bands to decrease to approximately 1/2 their original intensity. As with Al_2O_3, the Al-O stretching frequencies are centered at 800 and 600 cm^{-1}. The broad 445 cm^{-1} absorption could be due to NiO. Other bands are centered at 2100, 1530, 1390, 1070 and 1000 cm^{-1}.

The 1530 and 1390 cm^{-1} bands are thought to be associated with the asymmetric and symmetric stretching vibrations of a carbonate-like species. However, their large intensity does not seem to be explainable in terms of only *in situ* $CO_3^=$ generation. A number of tests were performed to clarify the origin of these, and other, bands.

First, the intensities of the 1390 cm^{-1} and 1520 cm^{-1} bands *vs* percent C150-4-03 in a KBr pellet were plotted, both for normally-pressed pellets and for pellets which have been pressed only after flushing with CO_2 for 15 minutes. These plots are shown in Fig. IV B3. The admission of CO_2 increased the intensity of these bands for all concentrations of C150-4-03, and the peak absorption frequencies and shapes remained constant. These facts indicate that non-linear CO_2 and/or CO_3 is held within the catalyst, being associated with either the Ni or Al.

Second, the spectra of $NiCO_3$ was obtained to determine whether a carbonate ion attached to Ni could generate the 1530 and 1390 cm^{-1} bands. As seen from Fig. IV B4 large spectral changes coincided with the heating of the $NiCO_3$ sample. If the 1475 and 1395 cm^{-1} bands are due to $CO_3^=$, it must be attached to the Ni as a unidentated ligand as depicted by(I). The

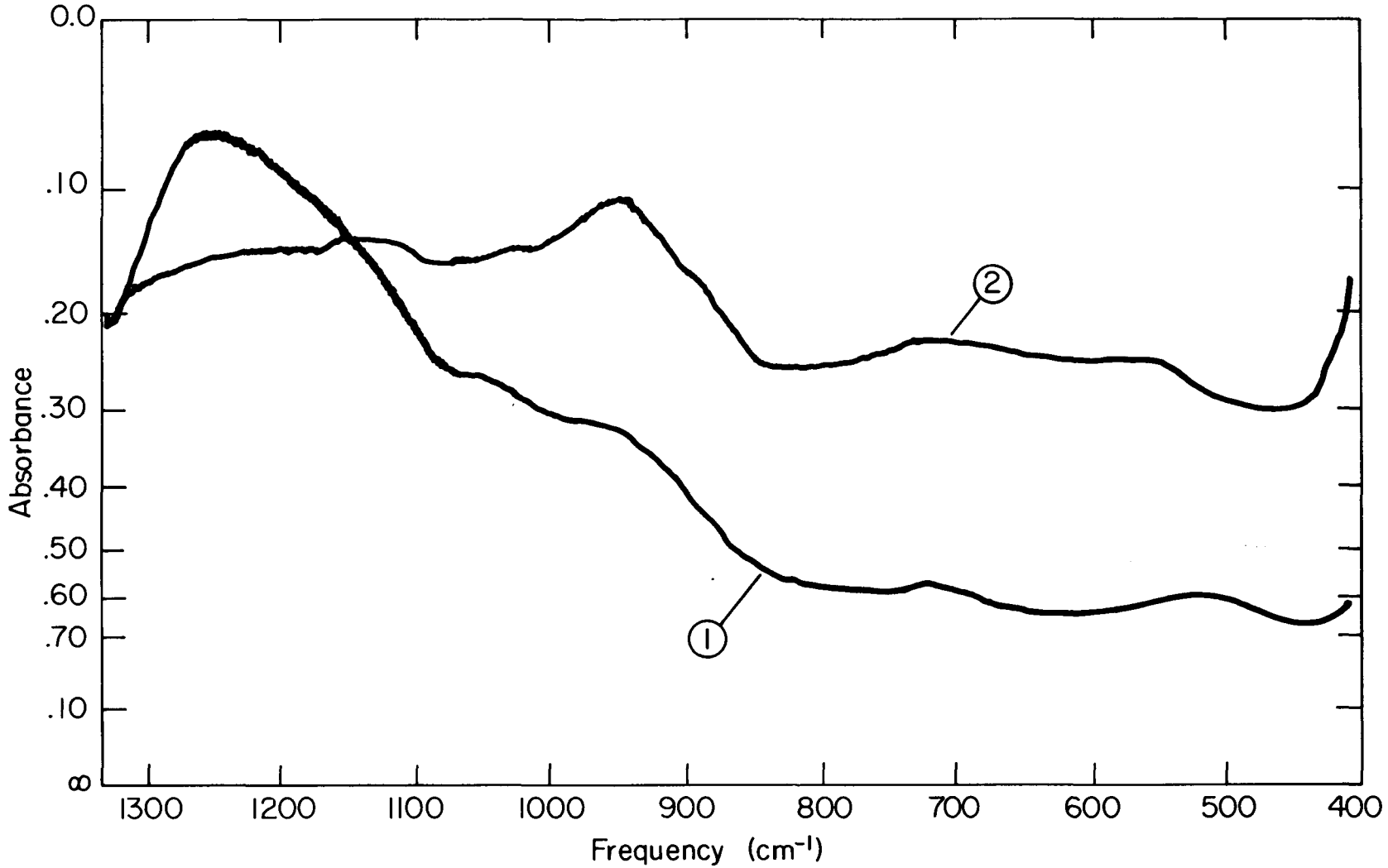

Fig. IV B2: (1) Infrared spectrum of C150-4-03 dispersed in a KBr pellet, 1300-400 cm^{-1}.
(2) C150-4-03/KBr pellet spectrum after heating at 300°C for 20 hours.

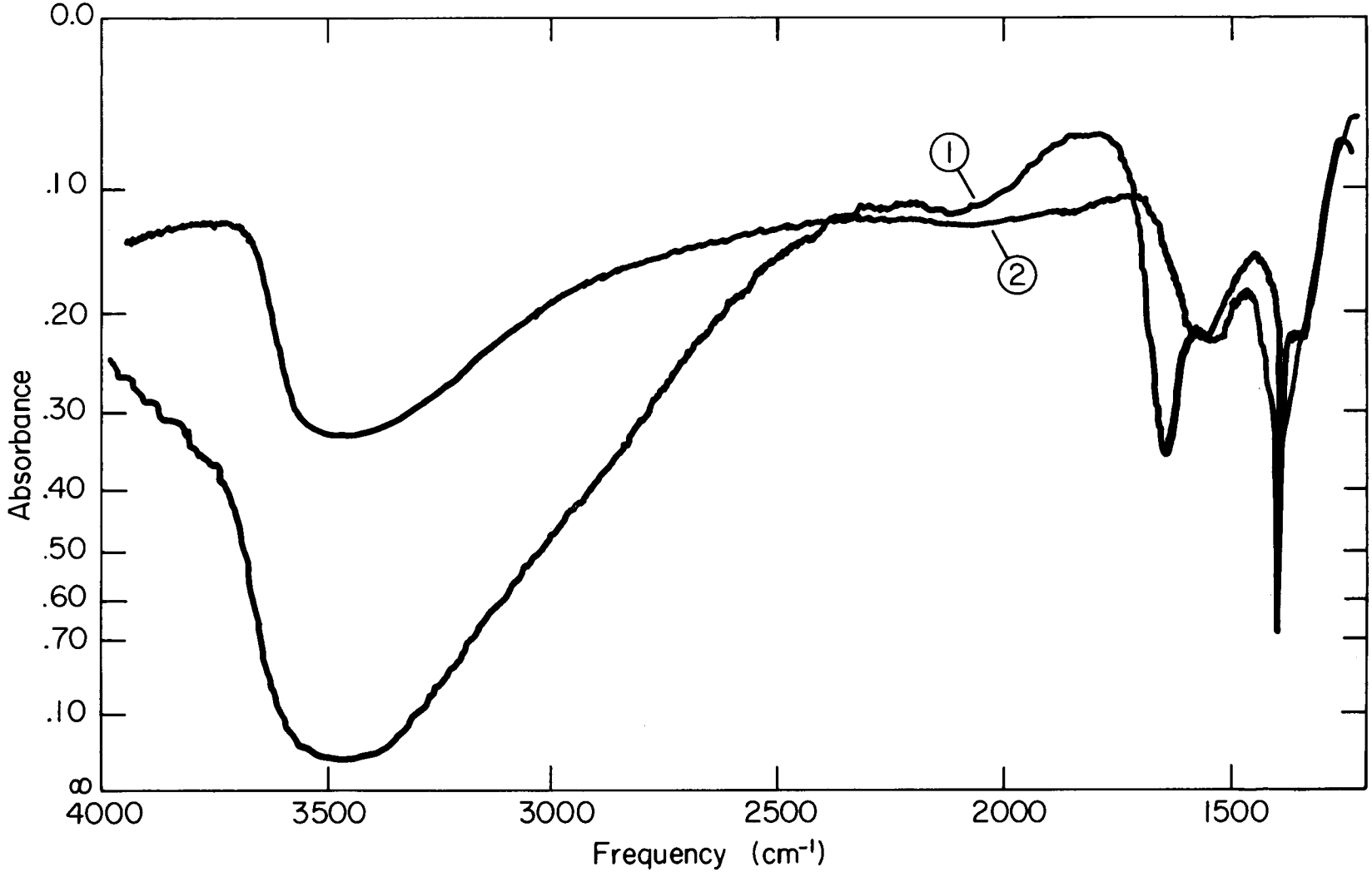

Fig. IV B2: (1) Infrared spectrum of C150-4-03 dispersed in a KBr pellet, 4000-1300 cm^{-1}.
(2) C150-4-03/KBr pellet spectrum after heating at 300°C for 20 hours.

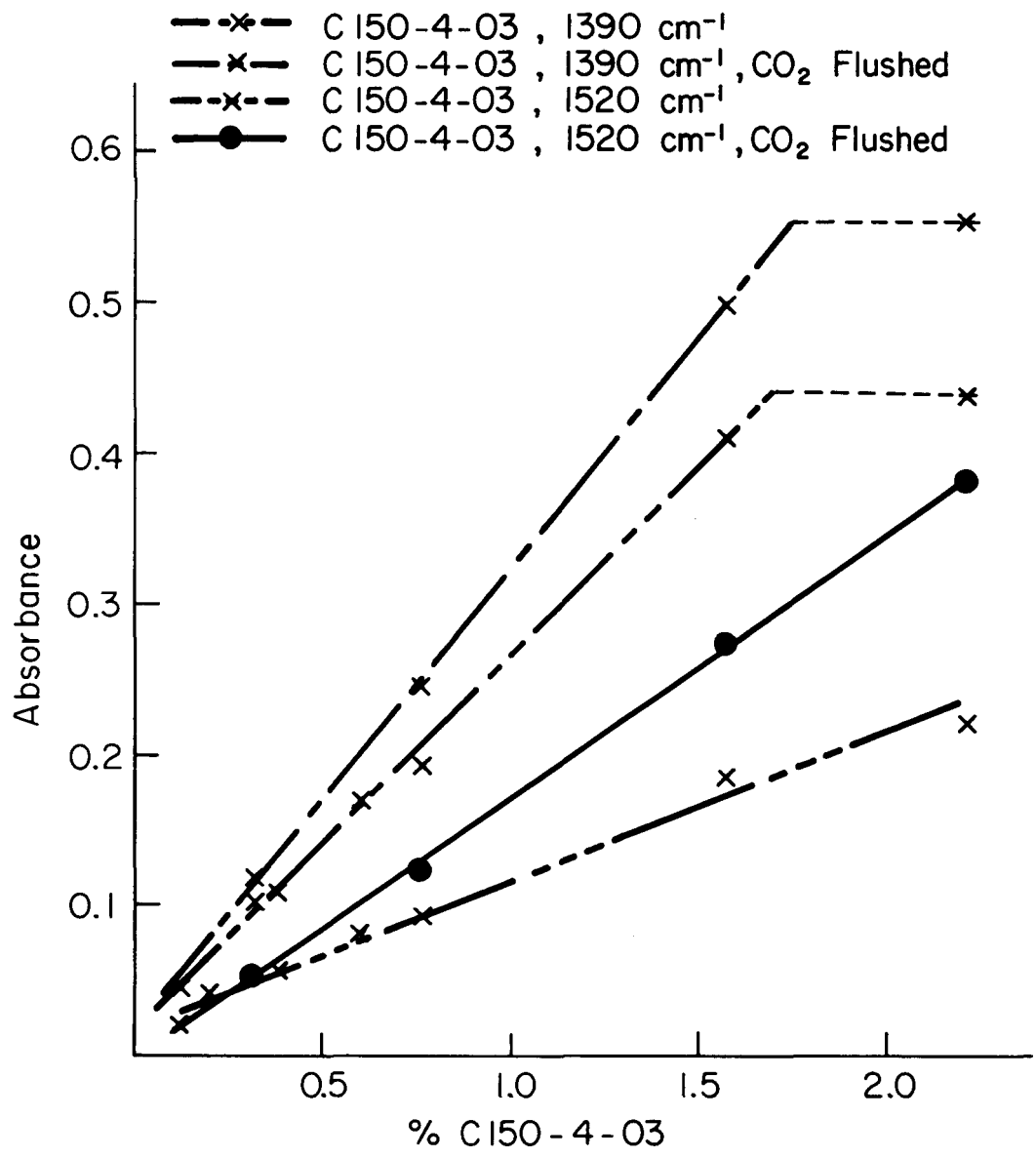

Fig. IV B3: Intensity of the 1520 and 1390 cm^{-1} bands versus the percentage of C150-4-03 in the KBr pellet.

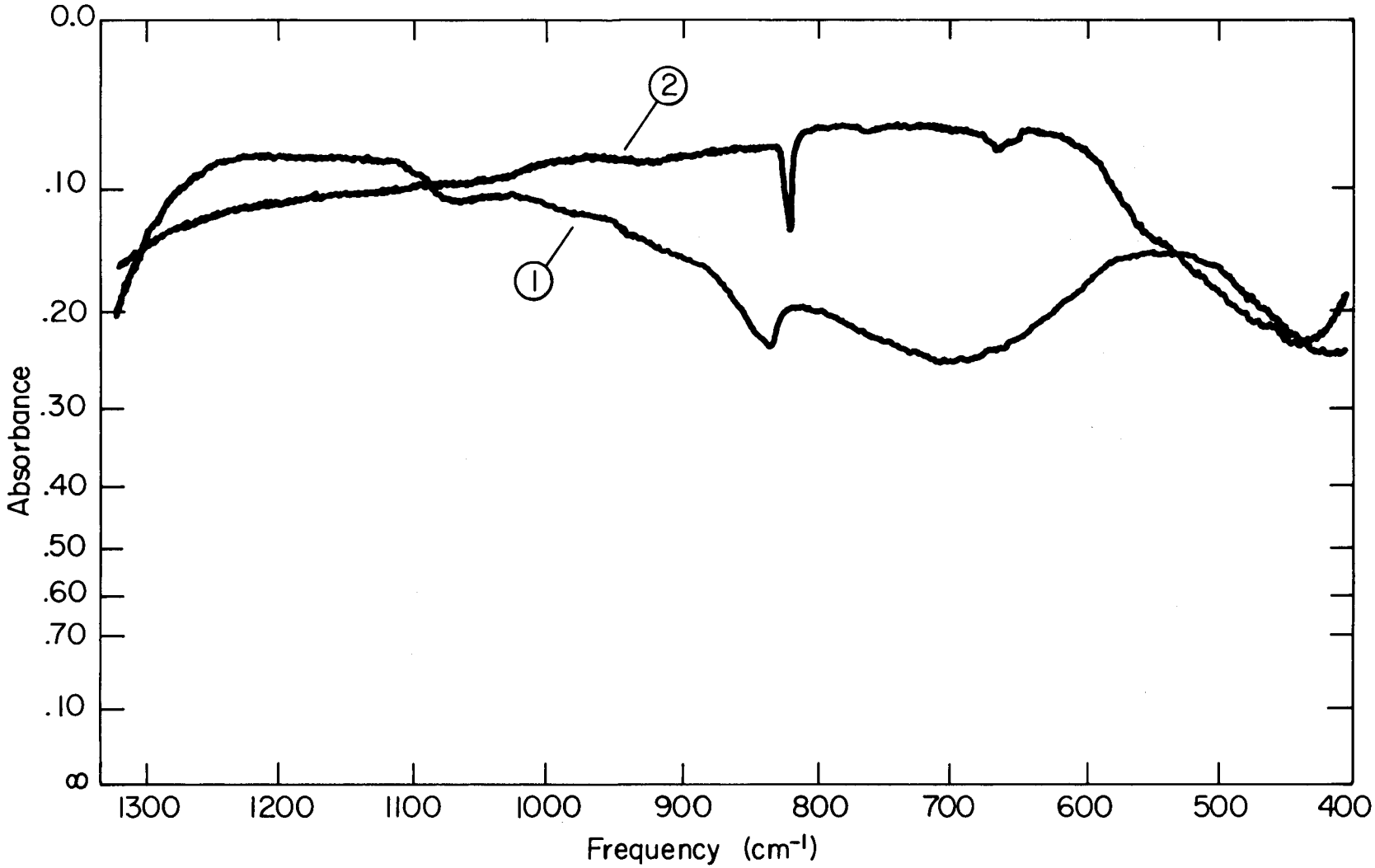

Fig. IV B4: (1) Infrared spectrum of $NiCO_3$ dispersed in a KBr pellet, 1300-400 cm^{-1}.
(2) $NiCO_3$/KBr pellet spectrum after heating at 300°C for 20 hours.

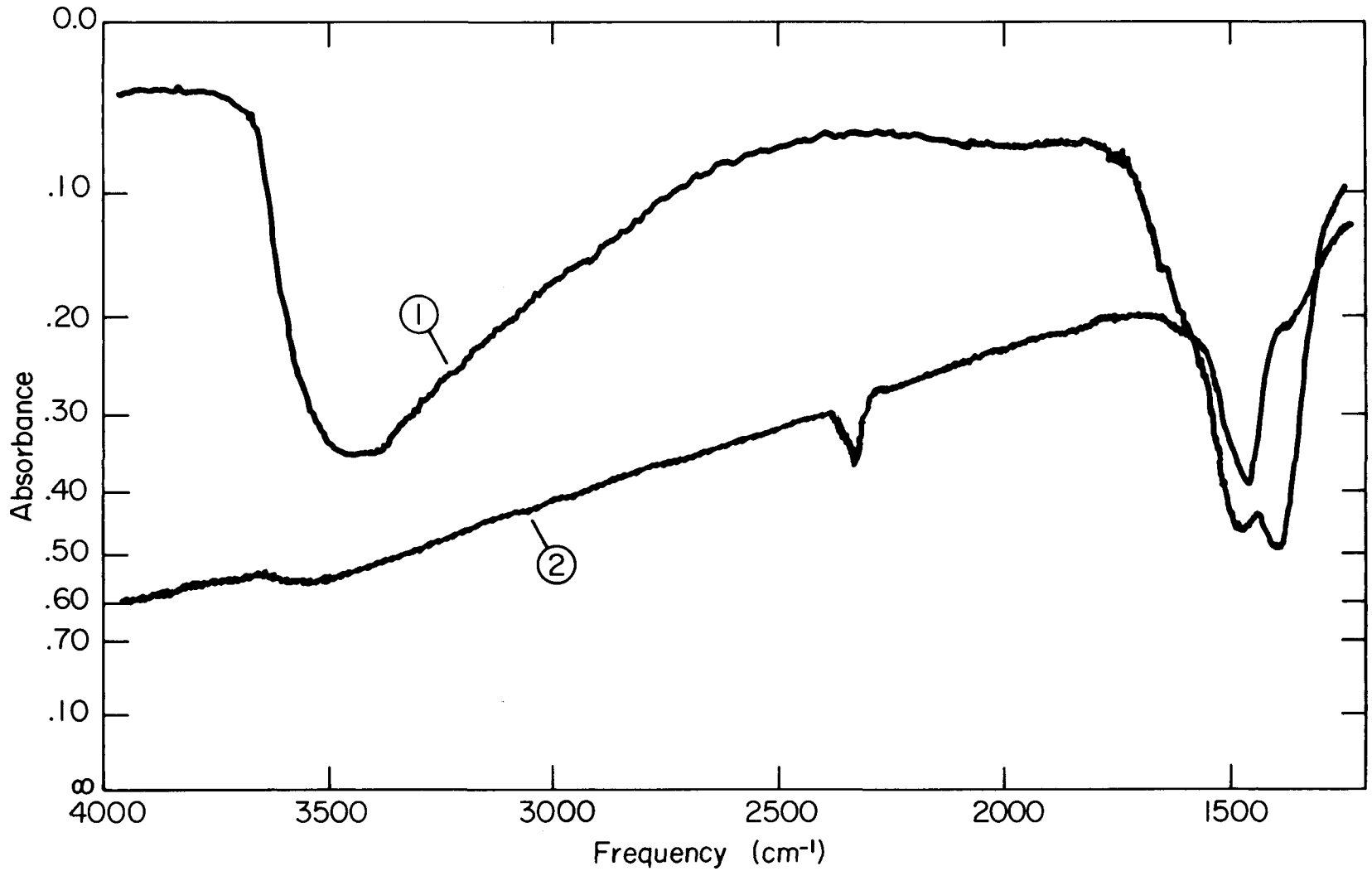

Fig. IV B4: (1) Infrared spectrum of $NiCO_3$ dispersed in a KBr pellet, 4000-1300 cm^{-1}.
(2) $NiCO_3$/KBr pellet spectrum after heating at 300°C for 20 hours.

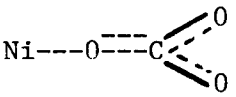

(I)

D_{3_h} symmetry of $CO_3^{=}$ attached to the Ni as shown by (II) would be expected to have absorption bands in the 1420, 860 and 680 cm^{-1} regions[7].

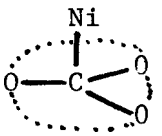

(II)

The 1395 cm^{-1} absorption which could be associated with a symmetric CO vibration for (I) as depicted by (III), would be infrared inactive for (II). Then the 1475 cm^{-1}

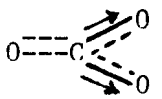

(III)

band would be the asymmetric vibration of species (III) while the weak 1070 cm^{-1} absorption would be the O---C stretching vibration and 870 cm^{-1} the out-of-plane bend of species (III).

As shown by Fig. IV B4 (2) the unidentate $CO_3^{=}$ ligand attached to Ni is unstable when heated to 300°C. The appearance of the 2340 and 670 cm^{-1} bands show the formation of linear CO_2 as the $NiCO_3$ decomposes. The remaining bands at 1475 and 820 cm^{-1} indicate that species (II) is formed, but only as an intermediate state to the total decomposition of the $NiCO_3$ which occurs with continued heating. This transitional molecule also shows characteristic Ni-C vibrations by the broadening of the 440 cm^{-1} band. Thus from this second step in analyzing the C150-4-03 spectra we find that the absorption frequencies of $NiCO_3$ do not coincide with those of the catalyst, and as shown previously, $NiCO_3$ decomposes quite readily with heating[8].

Third, the spectrum of $Na(OH)_2AlCO_3$ was obtained in order to compare the absorption frequencies in the 1400 cm^{-1} region. This spectrum is shown in Fig. IV B5 (1). It is to be compared with the corresponding C150-4-03 pressed pellet spectra of Fig. IV B5 (2) and with the same pellet spectra after the sample was heated at 300° for approximately 20 hours (Fig. IV B5) (3). The following characteristics are evident when comparing Fig. IV B5 (3) with IV B5 (2):

(1) A shift of approximately 50 cm^{-1} to 1570 cm^{-1} for the 1520 cm^{-1} band;

(2) No frequency shift for the 1390 cm^{-1} band;

(3) An initial decrease in the intensity of the 1390 cm^{-1} band, but continued heating at 300°C would not cause its disappearance;

(4) The appearance of a significant shoulder at 1350 cm^{-1}.

Fig. IV B5 shows very good correspondence between the $Na(OH)_2AlCO_3$ spectra and that of the catalyst. The shift of the 1520 cm^{-1} band with heating can be explained by a restructuring of the $CO_3^=$ with respect to the Al while the 1350 cm^{-1} shoulder could be due to the formation of $K_2[Al(CO_3)_2]Br \cdot {}_XH_2O$ (X is variable) or $Al_2(CO_3)_3$.[9] That the sharp 1390 cm^{-1} band is associated with the symmetric stretch of $CO_3^=$ is further strengthened by previous research [10] and by the spectra of C150-4-03 dispersed in CsI pellets. KBr forms a FCC crystalline lattice while CsI has a BCC lattice. The BCC lattice causes spreading of absorption bands due to free ions in solution.[11] We find that the 1390 cm^{-1} band spreads to an approximate 50 cm^{-1} width in CsI, while it has a 10 cm^{-1} width in KBr.

Fourth, we obtained the spectra of an alumina catalyst prepared by CCI which had only 10% Ni. The absorption band at 1390 cm^{-1} was 3.2 times more intense and the 1520 cm^{-1} band was 1.2 times more intense than the corresponding absorptions for C150-4-03. The discrepancy between these intensity increases for the asymmetric and symmetric stretching vibrations of $CO_3^=$ is not fully understood, but it may be related to the symmetry of the vibrations with respect to the KBr matrix.

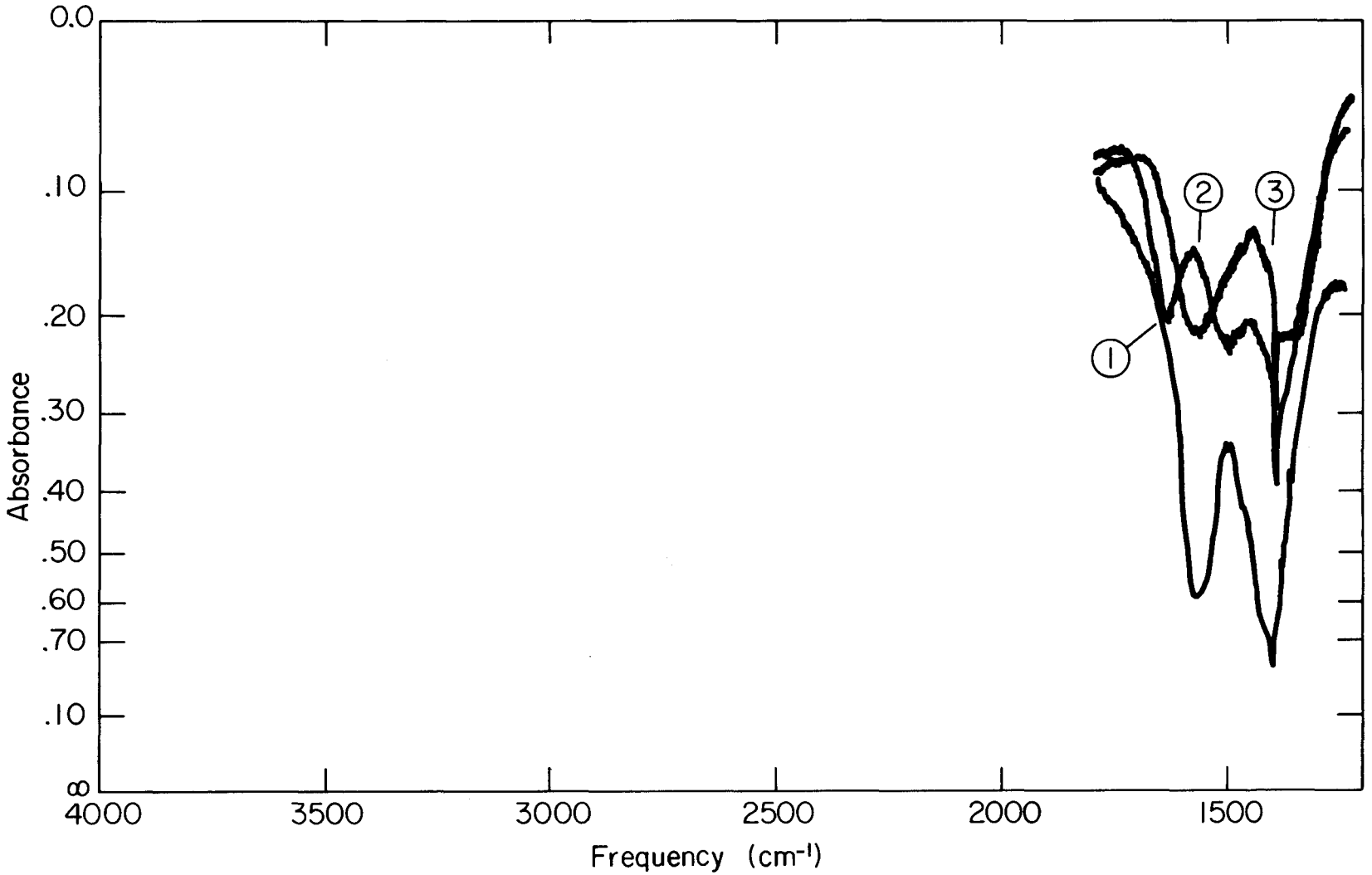

Fig. IV B5: Infrared spectrum of the CO_3 stretching region for (1) $Na(OH)_2AlCO_3$, and (2) C150-4-03, and (3) after the C150-4-03/KBr pellet was heated at 300°C for 20 hours.

C150-1-03

This is an alumina catalyst similar to C150-4-03. The infrared vibrational characteristics are almost identical to those of C150-4-03, and as such, will not be reproduced here.

SiO_2

The infrared spectra of SiO_2 was presented in the previous report[1]. Here we will assign its infrared bands and correlate these with the infrared spectra of the silica catalysts.

Upon comparing the solid SiO_2 spectra with published results [12, 13] we may assign the following:

1210 cm^{-1}	Si - O stretch
1110 cm^{-1}	Si - O stretch
810 cm^{-1}	Si - O - Si deformation
475 cm^{-1}	O - Si - O deformation

The 1210 cm^{-1} band is usually associated with SiO_2 complex, while bands in the 1100 cm^{-1} region are associated with SiO_3 complexes.[14] Although not evident in previous spectra, silicon compounds can absorb H_2O quite readily. When the corresponding KBr pellet is heated at 300°C a small absorption is apparent at 3675 cm^{-1}. This absorption is associated with the stretching vibration of OH^- groups attached to the Si atoms which can also give absorption in the 970 cm^{-1} region due to OH^- deformation vibrations[15].

$NiSiO_3$

This spectrum was given in the previous report. It is reproduced in Fig. IV B6 in order that it may be compared with the spectra of a sample heated to 300°C and to clarify some spectral details.

Fig. IV B6 (1) shows characteristic SiO_2 absorption at 1220, 800 and 470 cm^{-1}, along with SiO_3 absorption in the 1100 cm^{-1} region. The 670 cm^{-1} band is clearly shown to be a doublet upon heating at 300°C (ca. 710 cm^{-1} and 670 cm^{-1}). Likewise, heating causes the broad H_2O absorption at 3500 cm^{-1} to become a medium intense band at 3630 cm^{-1}, which still has a weak characteristic

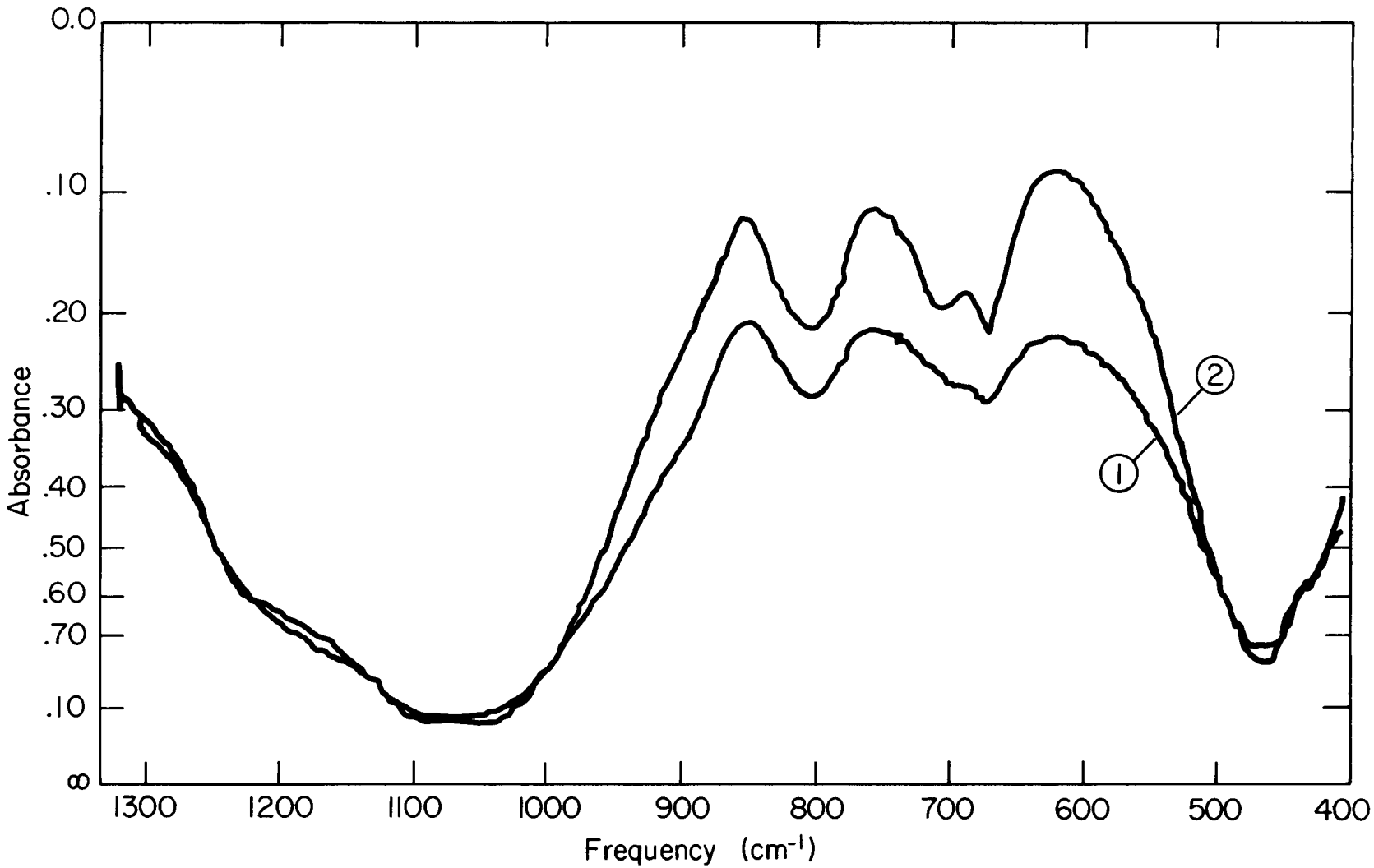

Fig. IV B6: (1) Infrared spectrum of "$NiSiO_3$" dispersed in a KBr pellet, 1300-400 cm^{-1}.
(2) "$NiSiO_3$"/KBr pellet spectrum after heating at 300°C for 20 hours.

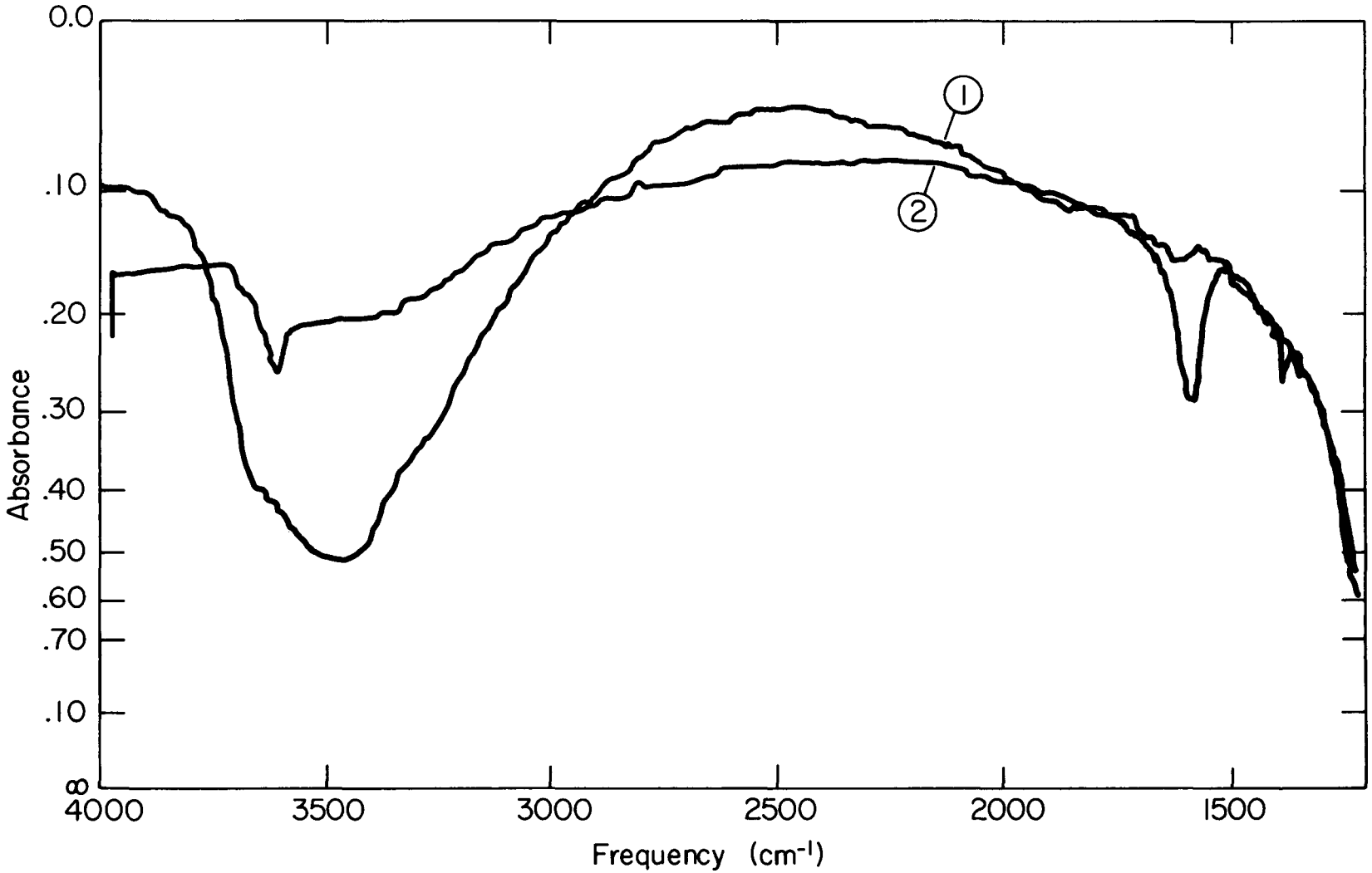

Fig. IV B6: (1) Infrared spectrum of "$NiSiO_3$" dispersed in a KBr pellet, 4000-1300 cm^{-1}.
(2) "$NiSiO_3$"/KBr pellet spectrum after heating at 300°C for 20 hours.

H_2O envelope. We find good agreement between Fig. IV B6 (2) and the absorption spectra of $Ni_4(OH)_2Si_2O_7$[16] for the 3630, 1070, 670 and 470 cm^{-1} regions. The 710 cm^{-1} band could then be explained in terms of $Ni^{+3}Si_2O_7$[16], with the 670-710 cm^{-1} doublet appearance due to the removal of excess-perturbing H_2O. The broad absorption from 1250 to 950 cm^{-1} could also be explained in terms of Si - O stretching vibrations for a mixture of compounds of the type SiO_2, SiO_3, Si_2O_7 and SiO_4. That a weak, narrow absorption appears at 1380 cm^{-1} is thought to be due to <u>in-situ</u> $CO_3^=$ generation.

<u>C150-1-01</u>

This is a "NiO/SiO_2" catalyst whose spectra is reproduced here in order that its spectral characteristics may be clarified. Fig. IV B7 (1) shows its infrared absorption when dispersed in a KBr pellet and Fig. IV B7 (2) shows the results of heating this pellet to 300°C.

There are considerable differences between the absorption frequencies of "$NiSiO_3$", SiO_2 and C150-1-01. The broad 3475 cm^{-1} band and the 1640 cm^{-1} in all cases are related to H_2O absorption. The only other band appearing at the same frequency for these compounds is 470 cm^{-1}. This is the O - Si - O bending vibration which will be relatively insensitive to the coordination of O to Si.

The low Si - O stretching frequencies (1060 and 1000 cm^{-1}) and the absence of a band at 800 cm^{-1}indicate that SiO_2 is not present in C150-1-01. Absorption at 1060 cm^{-1} is characteristic of (SiO_3) while that at 1000 cm^{-1} is characteristic of (SiO_4). The heating of the sample produces a more evident OH absorption at 3630 cm^{-1} while causing the appearance of bands at 2340 and 2185 cm^{-1}. The OH^- is tightly bound since continued heating at 300°C did not remove the band at 3630 cm^{-1}. This fact indicates the presence of $Ni_4(OH)_2Si_2O_7$, as for the "$NiSiO_3$" sample.[16] This would explain the 1060 cm^{-1} and 670 cm^{-1} absorptions.

Intense, narrow absorption at 1380 cm^{-1}, along with the weak shoulder at 1470 cm^{-1}, which shifts to 1510 cm^{-1} with heating, shows that a carbonate species is associated with C150-1-01 as it is for C150-4-03. This interpretation is strengthened by the appearance of the linear CO_2 stretching vibration at 2340 cm^{-1} for the heated sample. Evidently the $CO_3^=$ that is bound in the sample partially decomposes. It is not associated with the Ni, but

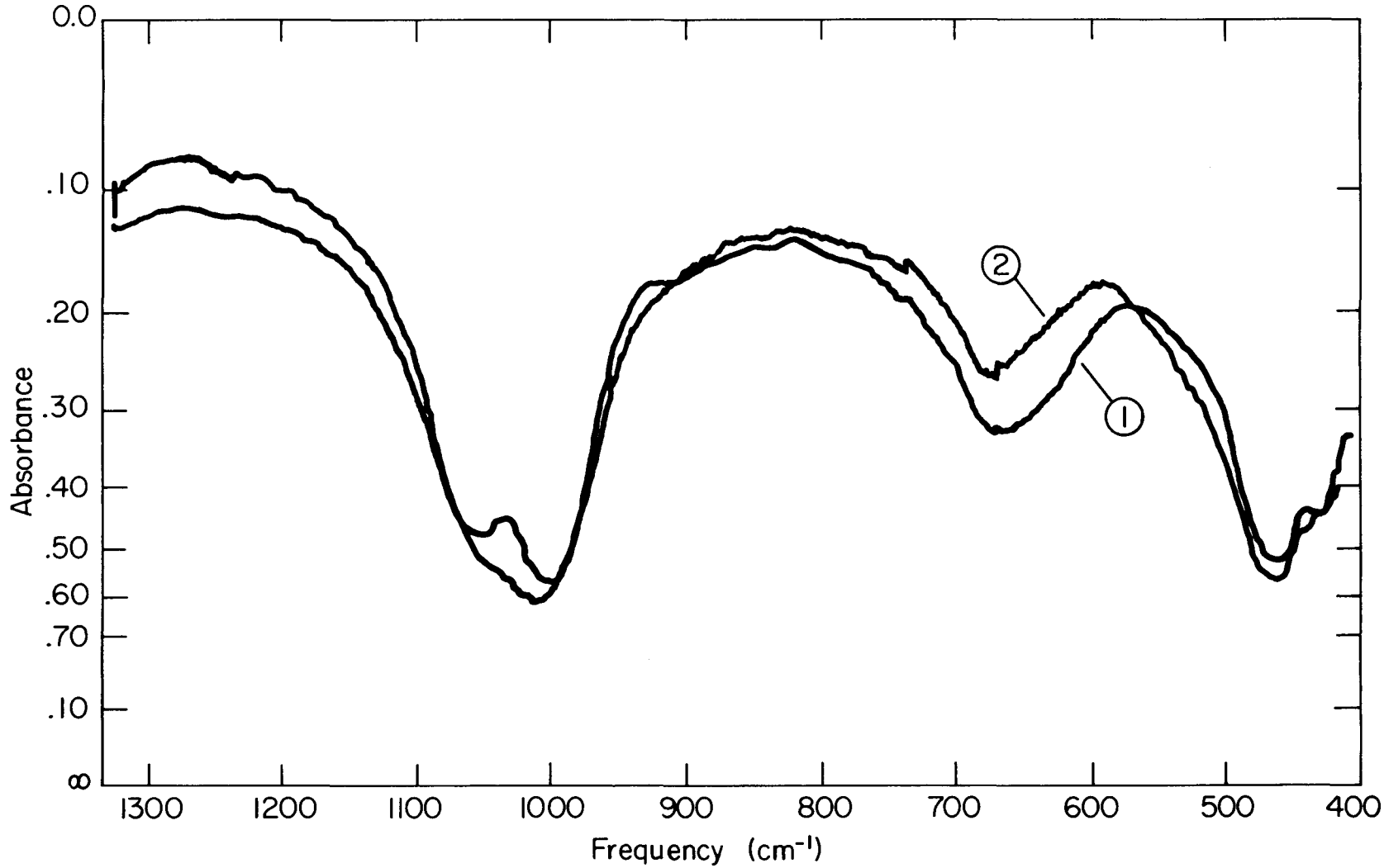

Fig. IV B7: (1) Infrared spectrum of C150-1-01 dispersed in a KBr pellet, 1300-400 cm^{-1}.
(2) C150-1-01/KBr pellet spectrum after heating at 300°C for 20 hours.

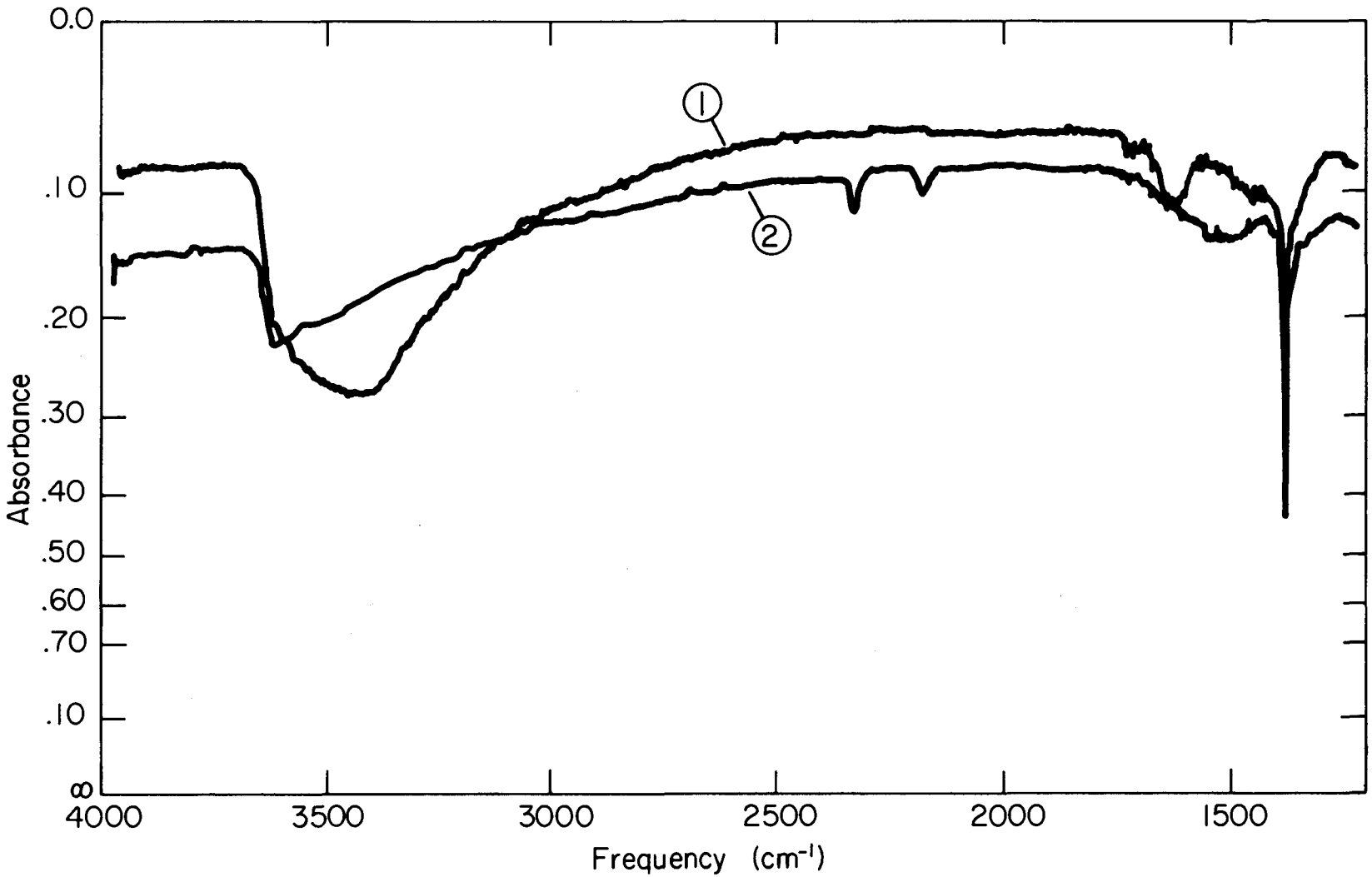

Fig. IV B7: (1) Infrared spectrum of C150-1-01 dispersed in a KBr pellet, 4000-1300 cm^{-1}.
(2) C150-1-01/KBr pellet spectrum after heating at 300°C for 20 hours.

primarily locked in the silicate lattice. The bending vibration of this species would also increase the 670 cm^{-1} band intensity as compared to that found for the "$NiSiO_3$" sample.

Other spectral details evident are an absorption at 440 cm^{-1} which is due to the Ni - O stretch, and weak absorption at 2185 and 900 cm^{-1}. The latter two are due to Si - H vibrations.[17-18]

C150-1-02

The infrared spectra of this Nickel-Silica catalyst is shown in Fig. IV B8 (1) and the heated sample spectra is shown in Fig. IV B8 (2). The spectral characteristics are very similar to C150-1-01. The main difference is the appearance of a very weak absorption at 2920 cm^{-1} for the heated sample. This is a C-H stretching frequency and could be caused by the production of $HCO_3^=$ induced by heating.

(ii) Work Forecast

The construction of the Raman cell for the investigation of single-crystal nickel samples is proceeding in our shop, but shipping delays in vacuum equipment ordered early last summer have caused a reordering of topics of investigation. We plan to (a) obtain and interpret the infrared spectra of the catalysts which have been sulfided, and (b) obtain and interpret the far infrared spectrum of all catalysts, including ones which have been sulfided. We expect to learn additional information on fundamental vibrational frequencies and on bonding. These catalysts are expected to have some fundamental modes of vibration below 400 cm^{-1}. Also, the low frequencies are often very sensitive to changes in force constants should such changes occur in sulfided catalysts.

The high-power Argon ion laser is to be shipped in about three weeks. It will be installed and the Raman spectrograph recalibrated. Then we will begin the Raman studies of the catalysts both before and after they are exposed to sulfur.

(iii) References

1. P. J. Reucroft, E. B. Bradley, R. J. De Angelis and G. A. Sargent. Quarterly Report No. 2, "Surface Structure and Mechanisms of Gasification Catalyst Deactivation," May 1 to July 31, 1976, ERDA Contract NO. E(49-18) 2229. p. 28.

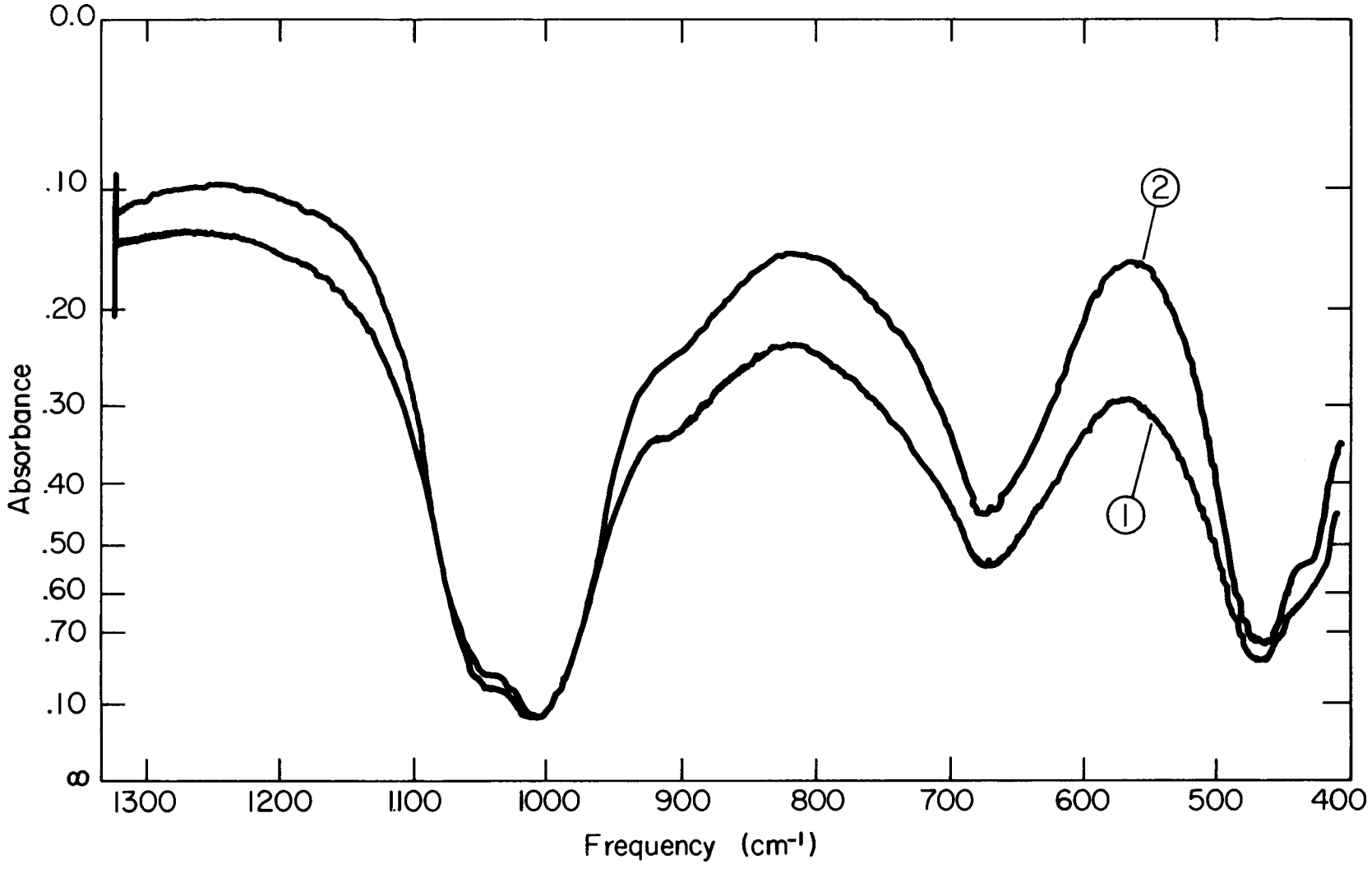

Fig. IV B8: (1) Infrared spectrum of C150-1-02 dispersed in a KBr pellet, 1300-400 cm^{-1}.
(2) C150-1-02/KBr pellet spectrum after heating at 300°C for 20 hours.

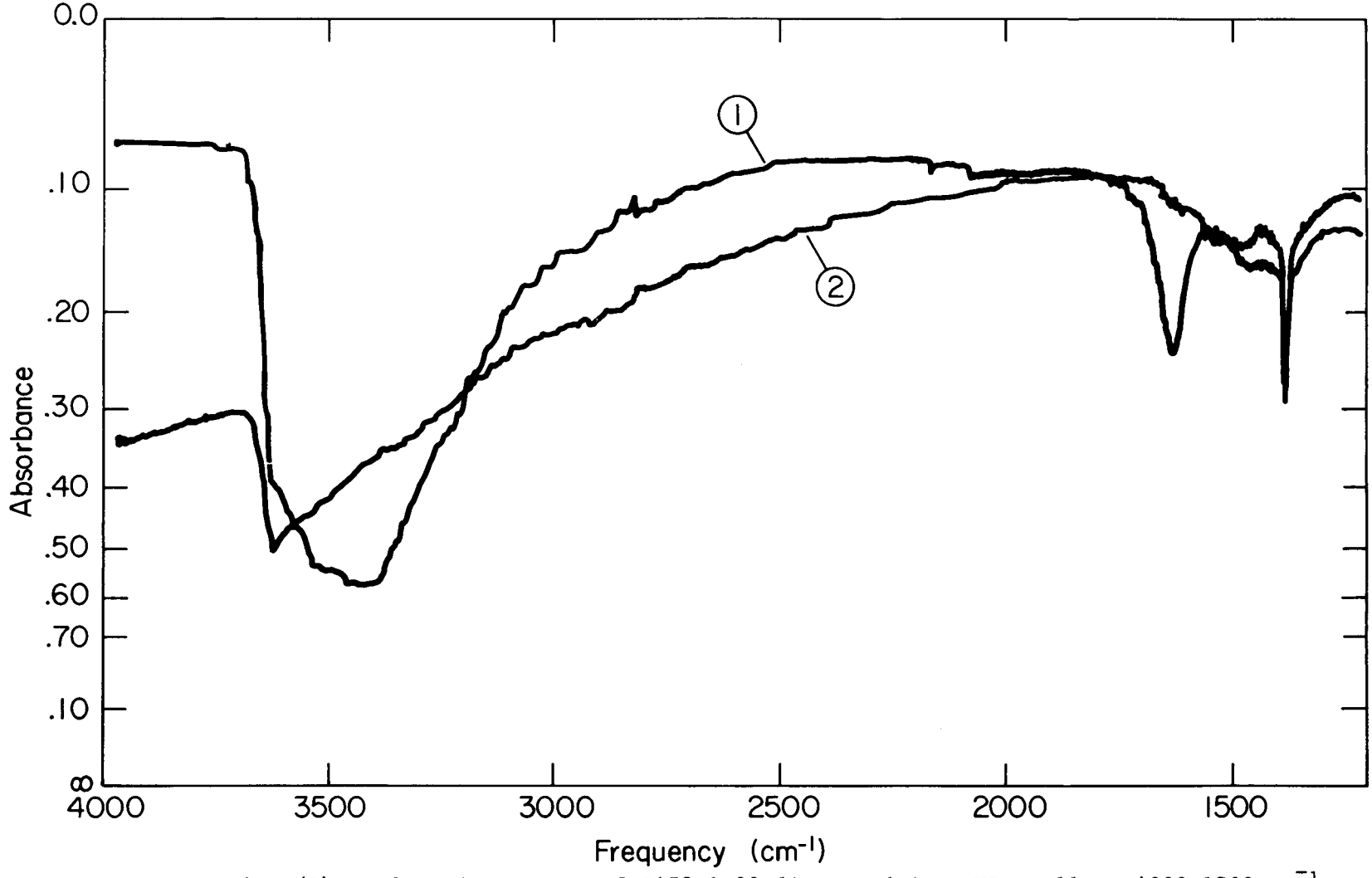

Fig. IV B8: (1) Infrared spectrum of C150-1-02 dispersed in a KBr pellet, 4000-1300 cm^{-1}.
(2) C150-1-02/KBr pellet spectrum after heating at 300°C for 20 hours.

2. P. J. Reucroft, E. B. Bradley, R. J. De Angelis and G. A. Sargent. Quarterly Report No. 2, "Surface Structure and Mechanisms of Gasification Catalyst Deactivation," May 1 to July 31, 1976, ERDA Contract NO. E(49-18) 2229. pp. 28, 33.

3. A. Mitsuishi, H. Yashinaga, S. Fujita and Y. Suemoto, Jap. J. Appl. Phys. 1, 1 (1962).

4. V. A. Kolesova, Optics and Spectroscopy, 6, 20 (1959).

5. P. Tarte, Spectrochim. Acta, 23A, 2127 (1967).

6. I. I. Plyusnia, J. Appl. Spec. 20, 214 (1974).

7. L. H. Little, Infrared Spectra of Adsorbed Species, (Academic Press, 1966), p. 76.

8. J. R. Lawson, N. Fuson and J. O. Le Flore, Infrared Spectra of Inorganic Polyatomic Ions in Solid Solution, (1965) spectra 68.

9. B. M. Gatehouse, S. E. Livingstone and R. S. Nyholm, J. Chem. Soc. 3137 (1958).

10. P. J. Reucroft, E. B. Bradley, R. J. De Angelis and G. A. Sargent. Quarterly Report No. 2, "Surface Structure and Mechanisms of Gasification Catalyst Deactivation," May 1 to July 31, 1976, ERDA Contract NO. E(49-18) 2229. p. 33.

11. H. Bonadeo and E. Silberman, J. of Mol. Spec. 32, 214 (1969).

12. D. M. Karpinos and S. P. Listovnichaya, V. Ya. Aivazov Porash, Met. 12, 71 (1972).

13. C. H. Perry and J. D. Wrigley, Jr., Appl. Opt. 6, 586 (1967).

14. I. I. Plyusnina, Zhur. Strukt. Khim. 2, 330 (1961).

15. A. U. Kiselev and V. I. Lygen, Infrared Spectra of Surface Compounds (John Wiley and Sons, 1975), p. 82.

16. P. H. Gaskell, Phys. and Chem. of Glasses, 8, 69 (1967).

17. C. H. Tindal, J. W. Straley and H. H. Nielsen, Phys. Rev. 62, 151 (1942).

18. G. E. Becker and G. W. Gobelli, J. Chem. Phys. 38, 2942 (1963).

C. REPORTING CATEGORY 3 - SURFACE ANALYSIS BY LOW ENERGY ELECTRON DIFFRACTION (LEED) AND AUGER ELECTRON SPECTROSCOPY (AES) (Prepared by C. H. Huang and G. A. Sargent)

(i) Work Accomplished.

The apparatus for LEED (Low Energy Electron Diffraction) and Auger Electron Spectroscopy studies was received on October 14, 1976. Installation and wiring of the system were accomplished by the end of October. Performance of the apparatus was then inspected. Several malfunctions in the apparatus components such as the PAR 128A Lock-In Amplifier, the 971-1008 Dual Range Ionization Gauge, and the CMA (cylindrical mirror analyzer) aperture control, have now been corrected. The Varian 981-2757A Scanning Sample Positioner will be replaced in the near future.

The system is now working in a satisfactory condition. The background pressure is currently 2.5×10^{-9} torr. It is anticipated that this pressure will be reduced to the low 10^{-10} torr region after bake-out of the main chamber.

To test the equipment performance, some preliminary studies have been carried out on a silicon single crystal. Fig. IV C1 shows the Auger Spectrum for a single crystal silicon specimen before cleaning the surface (the crystal was allowed to equilibrate in the chamber at 2×10^{-9} torr over the weekend). The 88 eV peak is due to a LMM transition of silicon, the 271 eV peak is due to a KLL transition of carbon, and the 508 eV peak is due to a KLL transition of oxygen. Fig. IV C2 shows the Auger Spectrum of the same silicon crystal after heating to ~950°C for 30 seconds. By comparing Fig. IV C1 and Fig. IV C2, several features of the Auger technique are clearly shown:

(1) The silicon peak, after cleaning, is about an order of magnitude more intense than that of the uncleaned Si, which is presumably covered by several monolayers of adsorbed impurity. The result illustrates the strong damping for Auger electrons with respect to depth. This character has made Auger Electron Spectroscopy one of the most sensitive surface techniques.

(2) The carbon peak shape before and after cleaning is different. This is due to the different chemical status of the carbon before and after cleaning. The carbon peak in Fig. IV C1 has the character of CO, while that in

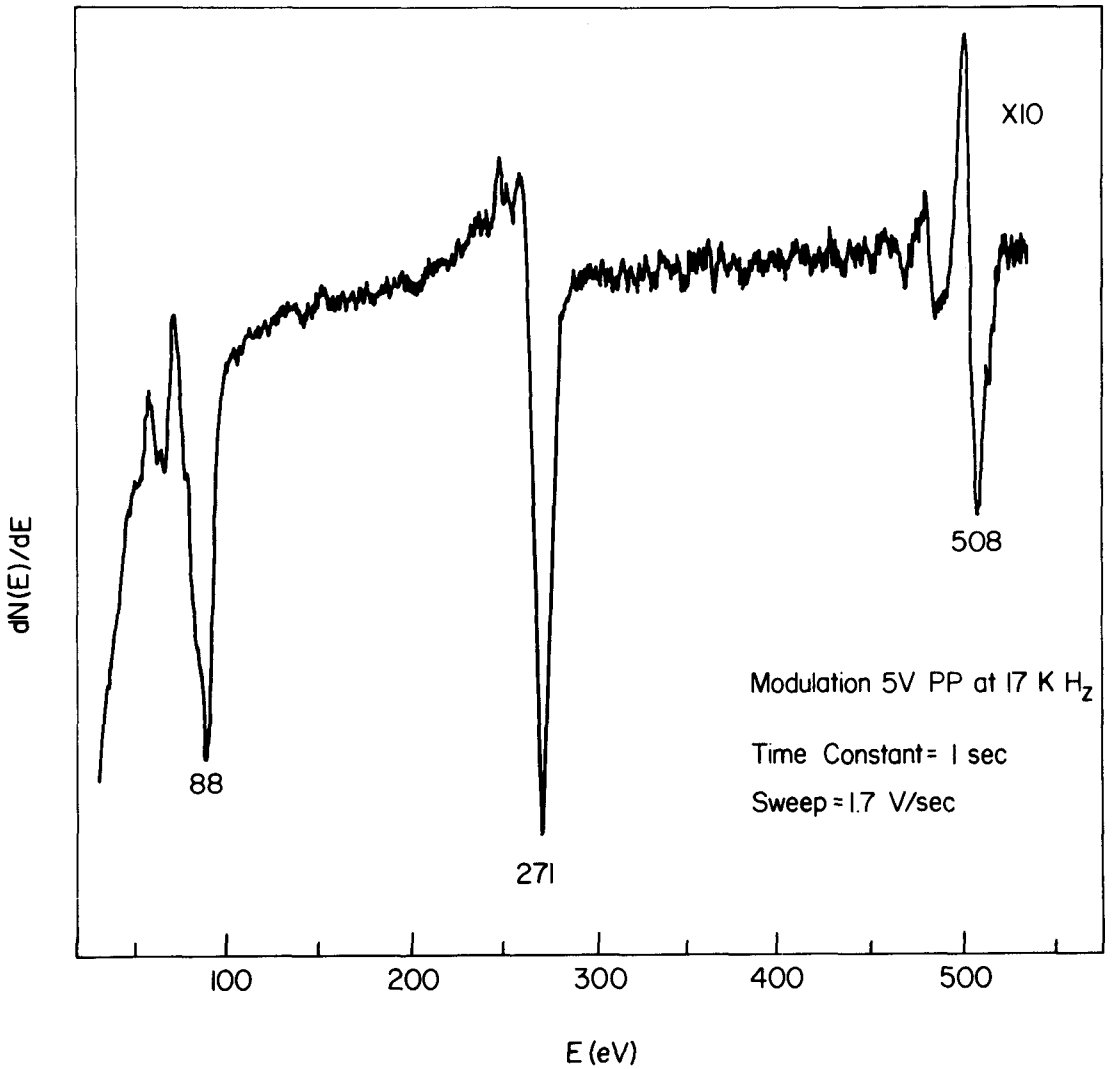

Fig. IV C1: Auger spectrum for a silicon single crystal before cleaning surface

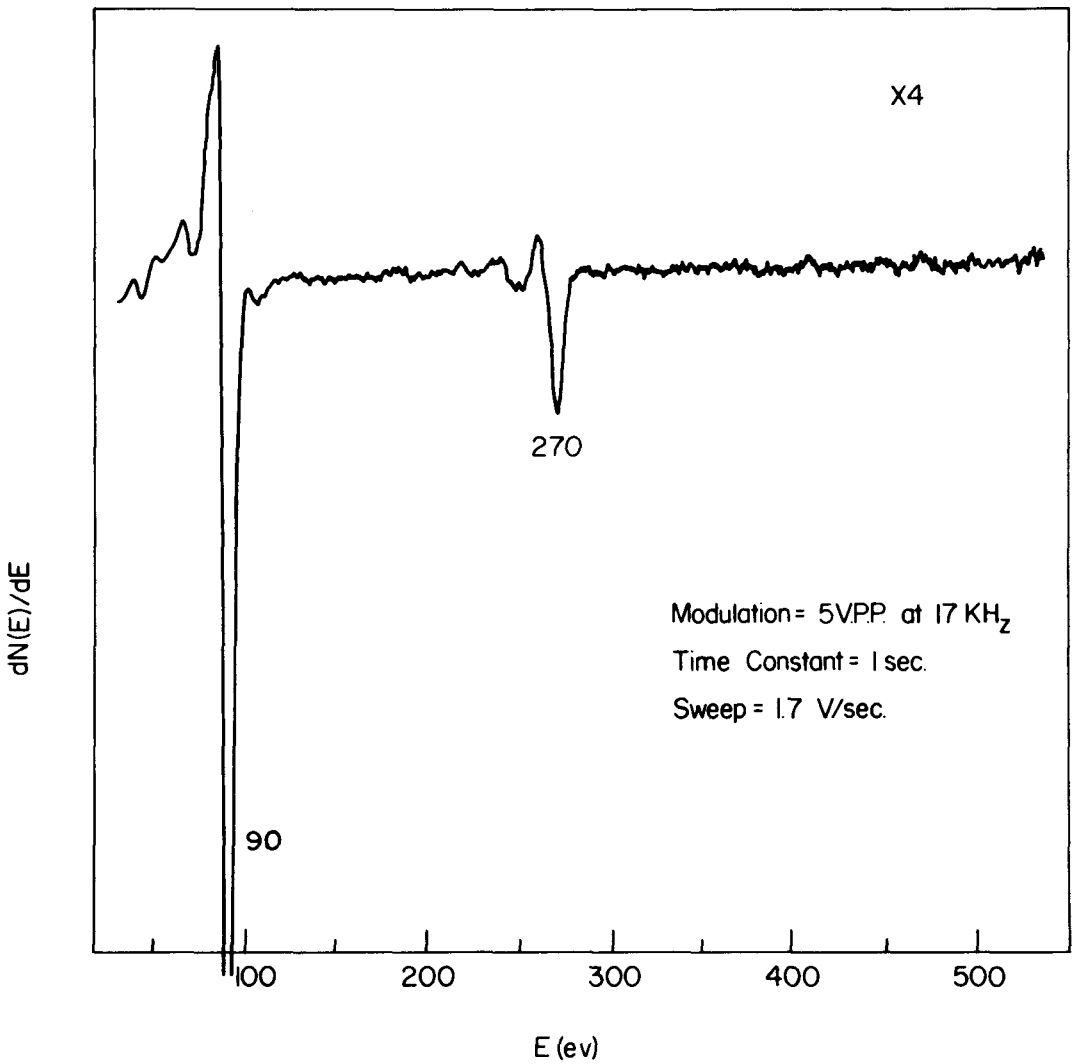

Fig. IV C2: Auger spectrum for a silicon single crystal after heating to 950°C for 30 seconds.

Fig. IV C2 is similar to the carbon peak observed in SiC[1]. The former peak is due to the adsorption of CO in the background pressure which is present in the chamber. The latter peak is possibly due to diffusion of carbon from the bulk of the silicon crystal to the surface or due to the decomposition of CO at the surface when the sample was heated. Thus, analysis of the peak shape can yield useful information on the binding state of the adsorbate.

(3) Shift of the Auger peak minimum: This shift should not be regarded as the chemical shift. Changes in chemical binding states also affect the shape of the N(E) vs. E curve (No. of Auger electrons vs. energy). Thus the shift of the minimum in $\frac{dN(E)}{dE}$ vs. E is not necessarily the same as the shift of the maximum of N(E) vs E. The Si Auger peak minimum for the heated Si is 2 eV higher in energy than that observed for the unheated sample, while the carbon peak on the cleaned silicon is 1 eV lower than that of uncleaned silicon.

Fifth order and seventh order structures of clean Si (111) (similar to those observed by J. J. Lander and J. Morrison at Bell Lab.[2]) were also observed after a brief and a lengthy heating of Si (111). Such surface reconstruction is one of the major factors which can determine the surface characteristics of crystalline solids and could be important in catalysis.

Calculation of LEED Intensities

In the previous report[3] it was mentioned that the computational schemes to describe the diffracted intensity theoretically as developed by Pendry[4] will be adopted. The adoptations of the LEED computer programs as written by Pendry[4] to our computer facilities have been quite successful and we have been able to reproduce the output of his sample set of typical data appropriate to a LEED calculation.

(ii) Work Forecast

(a) Modification of the Varian System: The system is a commercial product and several installations and modifications are necessary in order to meet our requirements for catalytic and chemisorption studies:

(1) The thermocouple gauge (gauge #1) was installed using teflon tape. It will be replaced with mini-conflat flange coupling in order to maintain the purity of the same gas in the manifold.

(2) An effusion source will be installed at the sample plane, so that the amount of gas introduced to the sample crystal can be accurately controlled while maintaining the ambient pressure and impurities at minimum levels.

(3) Installation of a gas inlet system: Three 1ℓ research grade gases (CO, H_2 and O_2) will be installed into the manifold through a covar seal. Also, 1ℓ of research grade argon will be installed directly to the main chamber through a bakeable leak valve. The argon is for ion etching purposes.

(b) Preliminary Study: The chemisorption and co-adsorption studies will be delayed pending the availability of a residual gas analyzer. However, our attention at the present time will focus on the elemental composition vs depth for a few commercial Ni catalysts such as the nickel on silica catalyst (C-150-1-01 R + S); or the nickel on alumina catalyst (C-150-4-03), etc. This will be done by monitoring the surface elements with the Auger technique and continuously etching the surface with Argon ions.

(c) Preparation of Ni (100), Ni (110) and Ni (111): Ni single crystals will be aligned and cut to within 0.25° of the above orientations, and then polished mechanically followed by chemical etching to remove foreign material. The finished crystal should be about 6 mm in diameter and 1/4 mm thick.

(d) Work function measurement: Surface potential changes can reveal the adsorbate coverage as well as its binding states. Thus work function measurement is an important technique in surface studies. A retarding potential technique will be employed for the contact potential difference measurement.

(iii) References

1. T. W. Haas, J. T. Grant and G. J. Dooley III, J. Appl. Phys. 43 1853 (1972).
2. L. H. Germer, Sci. American 212, 32 (1965).
3. P. J. Reucroft, E. B. Bradley, R. J. De Angelis and G. A. Sargent, Quarterly Report No. 2, "Surface Structure and Mechanisms of Gasification Catalyst Deactivation," May 1 to July 31, 1976, ERDA Contract No. E(49-18) 2229.
4. J. B. Pendry, "Low Energy Electron Diffraction - The Theory and Its Application to Determination of Surface Structure," Academic Press, (1974).

D. REPORTING CATEGORY 4 - X-RAY DIFFRACTION CHARACTERIZATION OF CATALYST MATERIALS (Prepared by P. Ganesan and R. J. De Angelis)

(i) Work Accomplished

The major objective of this work is to develop a reliable method to measure the particle size distribution function of a supported metal catalyst using x-ray diffraction profile shape analysis. Data of this type are required to test the existing catalyst sintering models. The method of analysis following Warren requires two orders of the diffraction profile[1] in order to separate the particle size and strain contributions to broadening of the x-ray line. In the case of supported metal catalysts it is not possible to obtain two orders of a (hkl) profile, therefore, in the work reported previously it was necessary to assume that the existing strains were zero in order to compute the particle size distribution function. The distribution functions obtained in this manner were included in the preceding report[2].

In this reporting period, an improved method of computation of the particle size distribution function from a single profile is reported. In this method, the zero strain assumption is eliminated. Results obtained in this period also indicate that the strains present in the supported metal catalysts (nickel oxide on alumina and silica) are very significant and must be taken into account in the computations.

Single Profile Analysis Technique

The single diffraction profile technique is based on the work of Gangulee[3] and Mignot[4]. Stokes corrected cosine coefficients[5] from a (hkl) diffraction profile are composed of two components, a size coefficient, A_L^S and a microstrain or distortion coefficient A_L^D; their relationship can be expressed as[2]:

$$A_L = A_L^S \cdot A_L^D \qquad (1)$$

where A_L are the Stokes' corrected cosine coefficient at L; where L is $n\delta$. Here n is the harmonic number and δ is a distance whose magnitude is inversely proportional to the fourier interval and L is a real distance normal to the diffracting planes. Defining a variable $x = 1/D_e$, where D_e is the effective

diffracting particle size, for small values of n and δ where the values of L are small and such that the number of diffracting domains in the specimen with this dimension is insignificant, the particle size term of the Fourier coefficients can be expanded as:

$$A_L^S = (1 - LX) \tag{2}$$

The distortion coefficient can be expanded for small values of n, as:

$$A_L^D = (1-KL^2\langle\varepsilon^2_L\rangle) \tag{3}$$

where K is $2\pi^2/d^2$, d is the (hkl) planar spacing and $\langle\varepsilon^2_L\rangle$ is mean square of the microstrain averaged over all distances in the diffracting specimen spaced L apart.

Letting $Y_L = K\langle\varepsilon^2_L\rangle$, the small L value cosine coefficient can be written as:

$$A_L = (1-LX)(1-Y_L L^2) \tag{4}$$

The Eq. (4) can be solved for X if the functional form of Y_L is known. In this way the particle size can be separated from the microstrain terms. The problem then resolves to determination of the most suitable forms of Y_L. Rewriting Eq. (4) gives,

$$A_L = 1 - LX - Y_L L^2 + XY_L L^3$$

Assuming the form of the strain function to be [6]:

$$Y_L = (C/L)\ \delta K \tag{5}$$

leads to an expression for A_L of:

$$A_L = 1 - L(X + C\delta K) + L^2(XC\delta K) \tag{6}$$

The expression for A_L has the form of a second order polynomial in L. Now defining a polynomial of second degree,

$$P_L = a_0 + a_1 L + a_2 L^2 \tag{7}$$

whose coefficients by comparison with Eq. (6) are:

$$a_0 = 1,\ a_1 = -(X + C\delta K) \text{ and } a_2 = (XC\delta K) \tag{8}$$

From these relationships it follows that,

$$X = 1/2\ (-a_1 \pm (a_1^2 - 4a_2)^{1/2})$$

$$D_e = 1/X$$

$$C = a_2|X\delta K \tag{9}$$

$$\langle \varepsilon^2_L \rangle = (C/L)\delta$$

The determination of the coefficients a_0, a_1 and a_2 can be made by solving the system of equations:

$$\sum_t A_L = a_0 N + a_1 \sum_t L + a_2 \sum_t L^2$$

$$\sum_t LA_L = a_0 \sum_t L + a_1 \sum_t L^2 + a_2 \sum_t L^3 \tag{10}$$

$$\sum_t L^2 A_L = a_0 \sum_t L^2 + a_1 \sum_t L^3 + a_2 \sum_t L^4$$

where N is the number of coefficients used in the evaluation, N> 4; t is an integer satisfying $t = L_N - L_0/L_1 - L_0$, where L_0 is the distance corresponding to the initial coefficient used in the computation of Eqs. (10).

The best solution to Eqs. (10) are selected from four criteria

(1) $a_0 \simeq 1$

(2) $a_2 > 0$, since a_2 from Eqs. (6) and (7) can be written as d^2A_L/dL^2 which must be positive.

(3) $\sum_t (P_L - A_L)\ /N$ is a minimum

(4) $(dA_L/dL)_{L\to 0} = a_1 = -(X + C\delta K)$

After the best solution to Eq. (10) is determined it is a simple process to calculate the average coherent diffracting particle size D_e and lattice mean square strain $\langle \varepsilon^2_L \rangle$ by employing Eq. (9).

The effective particle size, D_e, obtained by single profile analysis for unreduced nickel oxide catalysts are reported in Table I, along with the particle size obtained from the half breadth of the profile and the initial slope of the Stokes' corrected coefficients of the profile. Also the values of the lattice microstrain $\langle \varepsilon_L \rangle$ obtained from this analysis are reported in the last column. It is evident that the strains are indeed quite appreciable and hence

cannot be neglected as was done in the previous analysis of the same data. Also the microstrains tend to decrease upon sintering.

An important point to be noted from the single profile analysis is the fact that it is impossible to obtain the particle size distribution function $\partial^2 A_L^S / \partial_L{}^2$, since from Eq. (2) $\partial^2 A_L^S / \partial_L{}^2$ reduces to zero. However, it is possible to obtain the particle size distribution function by combining both single profile and multiple order analysis in the following manner. The expression for the relationship between the particle size and distortion coefficients in the Warren-Averbach method [2] is given by:

$$A_L = A_L^S \langle \cos 2\pi \, L/d \, \varepsilon_L \rangle \tag{11}$$

For small values of L/d the argument of the microstrain term is small and Eq. (1) can be rewritten as:

$$\ell n A_L = \ell n A_L^S - 2\pi^2 \frac{L^2}{d^2} \langle \varepsilon^2{}_L \rangle \tag{12}$$

This method of separation of particle size and microstrain terms makes no assumption of the nature of strains and Eq. (12) is good only for small values of L/d. However, it can be shown[7] that Eq. (12) is exact for all values of L/d if the microstrain distribution is Gaussian. However it is possible to obtain the particle size coefficient A_L^S from Eq. (12) by substituting the values for mean square strain $\langle \varepsilon^2{}_L \rangle$, obtained from single profile analysis. The particle size distribution function can then be obtained by differentiating the plot of A_L^S versus L twice graphically. Such an analysis is under investigation at the present time.

(ii) Work Forecast

In the next reporting period, the computer code for the single peak method to obtain the particle size distribution function will be completed. Data on the as received catalysts along with the sintered catalysts will be processed to obtain the strain corrected particle size distribution functions.

(iii) References

1. B. E. Warren and B. L. Averbach, J. Appl. Phys., 21, 595 (1950).
2. P. J. Reucroft, E. B. Bradley, R. J. De Angelis and G. A. Sargent. Quarterly Report No. 1., "Surface Structure and Mechanisms of Gasification Catalyst Deactivation," February 1 to April 30, 1976, ERDA Contract No. E (49-18) 2229.

3. A. Gangulee, J. Appl. Cryst. 7, 434 (1974).
4. J. Mignot and D. Rondot, Acta Met., 23, 1321 (1975).
5. A. R. Stokes, Proc. Phys. Soc., 61, 382 (1948).
6. R. L. Rothman and J. B. Cohen, Advanc. X-ray Analysis, 12, 208 (1969).
7. B. E. Warren, Progress in Metal Phys., 8, 152 (1959).

TABLE I

Particle Sizes and Microstrains of Nickel Oxide Catalyst Materials as Measured by Various X-ray Diffraction Techniques

Catalyst No. (heat Treatment)	(220) Center of Gravity (2θ)	$D_{\text{half breadth}}$ (Å)	$D_{\text{coefficient}}$ (Å)	D_e (Å)	Microstrain $\langle \varepsilon^2_{200Å} \rangle^{1/2} \times 10^2$
C-150-1-01 Silica	60.95	32.37	20.8	20.4	0.40
C-150-1-02 Silica	65.24	41.92	21.0	22.0	0.60
C-150-1-03 Al_2O_3	62.64	27.48	18.4	19.5	0.57
C-150-4-03 Al_2O_3	62.95	43.30	24.5	25.8	0.77
C-150-1-01 (1000°C, 1 hr.)	62.61	108.	54.	48.	0.23
C-150-1-02 (1000°C, 1 hr.)	62.38	75.4	46.	50.	0.32
C-150-4-03 (900°C, 1 hr.)	62.37	170.	91.	88.5	0.19
C-150-4-03 (1000°C, 1 hr.)	62.46	204.2	103.	103.8	0.36

V. CONCLUSIONS

1. ESCA binding energy shifts due to surface charging appear to be ~1.5 eV in the case of nickel oxide standard samples.
2. ESCA binding energy shifts due to surface charging are higher in the case of Al_2O_3 (3.9 eV) and SiO_2 (3.3 eV) samples.
3. The oxygen ESCA spectra of nickel oxide standard samples confirm the two valence state character of these samples.
4. Problems associated with surface charging and sample re-oxidation greatly complicate the interpretation of the ESCA spectra obtained for the catalyst samples that have been investigated. The results indicate, however, that a significant fraction of the nickel in the reduced catalyst is present in chemical forms other than metallic nickel.
5. Lattice microstrains present in pre-reduced nickel catalysts (support material silica or alumina) are very large.
6. The magnitude of the microstrains detected in pre-reduced nickel catalysts, tends to decrease on sintering at 900°C and 1000°C.
7. Apparatus for low energy electron diffraction (LEED) and Auger Electron Spectroscopy (AES) has been received and installed. Calibration and testing of the equipment performance has been undertaken.
8. Computer modelling of the LEED diffracted intensities has been undertaken using the programs developed by Pendry.
9. The silica support in the C150-1-01 and C150-1-02 catalysts is not of the form SiO_2.
10. The spectral characteristics of the C150-1-01 and C150-1-02 catalysts are similar to those found for linear chain silicates.
11. OH^- is present and tightly bound in significant amounts in the C150-1-01 and C150-1-02 catalysts.
12. $CO_3^=$ is in the C150-1-01 and C150-1-02 catalysts and cannot be explained by in-situ generation.
13. $CO_3^=$ is bound in the silicate structure, and not to the Ni in the C150-1-01 and C150-1-02 catalysts.
14. The C150-4-03 catalyst has Al - O vibrations characteristic of tetrahedrally- or octahedrally-coordinated Al.

15. H_2O is tightly bound in the C150-4-03 catalyst.

16. The absorptions due to $CO_3^{=}$ in the C150-4-03 catalyst cannot be explained by only <u>in-situ</u> generation from atmospheric CO_2 and H_2O, but must be the result of residual $CO_3^{=}$ from the catalyst preparation.

17. $CO_3^{=}$ is associated with the Al and not the Ni in the C150-4-03 catalyst.

VI. ACKNOWLEDGMENTS

Catalyst samples and general information were supplied by A. L. Hausberger and associates at Catalysts and Chemicals, Inc., Louisville, Kentucky.

☆ U.S. GOVERNMENT PRINTING OFFICE: 1977-740-094/